NASA CONTRACTOR REPORT

NASA CR-450

RESPONSE OF COMPLEX SHELL STRUCTURES TO AERODYNAMIC NOISE

by Jerry W. Schweiker and Robert E. Davis

Prepared under Contract No. NAS 1-3179 *by*
MCDONNELL AIRCRAFT CORPORATION
St. Louis, Mo.
for Langley Research Center

NATIONAL AERONAUTICS AND SPACE ADMINISTRATION • WASHINGTON, D. C. • APRIL 1966

RESPONSE OF COMPLEX SHELL STRUCTURES TO AERODYNAMIC NOISE

By Jerry W. Schweiker and Robert E. Davis

Prepared under Contract No. NAS 1-3179 by
MCDONNELL AIRCRAFT CORPORATION
St. Louis, Mo.

for Langley Research Center

NATIONAL AERONAUTICS AND SPACE ADMINISTRATION

For sale by the Clearinghouse for Federal Scientific and Technical Information
Springfield, Virginia 22151 – Price $2.00

RESPONSE OF COMPLEX SHELL STRUCTURES TO AERODYNAMIC NOISE

By Jerry W. Schweiker and Robert E. Davis

SUMMARY

This report presents the results of a research study on the high frequency response of shell-type structures to a buffeting aerodynamic environment. The major emphasis has been on the development of a method for calculating the statistics of shell response due to aerodynamic noise. The basic matrix formulation of the response equations is developed. The aerodynamic input is discussed with particular emphasis on the use of statistically reduced wind tunnel pressure data. Various methods for obtaining the necessary vibration characteristics of the shell structure are presented. With flight acceleration data available from the Mercury/Atlas flights, calculated response data have been determined for comparison purposes. This comparison shows good agreement in predicting over-all response levels.

INTRODUCTION

The problem of structural response to buffeting flows excitation has been of considerable interest since a series of launch-vehicle failures occurred during the initial phase of the space program. This interest is illuminated by recent papers on the subject (References 1, 2, and 3). Consequently, not only have analytical studies been intensified, but more detailed "detective" work has been concentrated in the area of collating fluctuating pressure measurements from flight and wind tunnel tests. This, in turn, has led to better defined wind tunnel programs, and more efficient methods of data reduction. As an integral part of this research, NASA (Langley Research Center) supported a two year study by McDonnell Aircraft Corporation, the primary goal being a reasonable method of predicting the high frequency response of shell-type structures to fluctuating pressures resulting from buffeting flows.

The investigation of the shell response problem is logically resolved into three distinct phases: (1) definition of the aerodynamic excitation, (2) definition of the vibration characteristics of the structure (mode shapes, damping, generalized masses, and frequencies), and (3) development of the response equations. Each of these phases were investigated in considerable depth, not only as compartmentalized areas, but also from the standpoint of mutually compatible descriptions permitting the development of an over-all integrated approach for determining the shell response in a buffeting flow. Based on these investigations, an IBM 7094 program has been developed which will calculate the deflection and acceleration spectra of a shell-type structure excited by aerodynamic buffeting. This program accepts aerodynamic excitation input in the form of statistical data

reduced from wind tunnel tests with the option of including either theoretical or experimental vibration characteristics.

This report presents the final technical results and conclusions resulting from the two year research study. The aerodynamic aspects, shell vibration characteristics, and the response equations are covered in this sequence with an additional section included on comparison studies of flight and calculated acceleration data. Detailed analytical developments of the aerodynamics and response which are a direct result of this research are presented in References 4 and 5, whereas the IBM 7094 response program description is presented in Reference 6. The reduction of fluctuating pressure data from various wind tunnel tests are presented in References 7 - 11. In addition, Reference 12 presents a collation of fluctuating buffet pressures.

Special acknowledgment should be made to J. T. Weissenburger for his valuable contributions as project leader for the first year of this contract.

SYMBOLS

A	Surface area
A_m^n, B_m^n, C_m^n	Mode shape coefficients for displacements w, u, v, respectively
a, b	Panel dimensions in x, y direction, respectively
C	Co-spectrum, real part of S defined below
$\Delta C_{p_{rms}}$	Root-mean-square pressure divided by dynamic pressure
E	Modification factor (Equation A4)
F	Generalized force
f	Frequency in cycles per second
G	Function of frequency defined in text
g_{rms}	Root-mean-square radial acceleration divided by gravitational constant having same units
H	Function of frequency defined in text
i	$\sqrt{-1}$
L	Length of shell frustum
M	Generalized mass
m	Number of longitudinal half-waves of a given mode
N	Number of samples used to determine probability distribution
n	Number of circumferential waves of a given mode
p	Pressure
Q	Quad-spectrum, imaginary part of S defined below
q	Normal coordinate
q_d	Dynamic pressure
R	Auto-correlation or cross-correlation depending upon: (1) alike or unlike superscripts, or (2) alike or unlike variables within parenthesis
r	Radius of shell

S	Power spectrum or cross-spectrum depending upon: (1) alike or unlike superscripts, or (2) alike or unlike variables within parenthesis.
	Note: $S(\pm\omega)$, $S(\pm f)$ refers to the mathematical definition of the power spectral density functions defined over $(-\infty, \infty)$, whereas $S(\omega)$, $S(f)$ refers to the physical power spectral density functions defined over $(0, \infty)$.
x	(1) Coordinate defining distance along cone generator from apex to a point on shell or (2) panel coordinate.
y	Panel coordinate
T	Period of time over which spectral functions are determined, theoretically approaching infinity
t	Time
U_c	Convection velocity
U_∞	Freestream velocity
w, u, v	Radial, tangential, and circumferential displacements
Z	Reciprocal of complex frequency response function
α	Streamwise decay rate
$\bar{\alpha}$	Complement of conical shell half-angle
β	Circumferential decay rate
δ_{Kl}	Kronecker Delta
ζ	Ratio of damping to critical damping
η	Defined in text
θ	Coordinate defining angular position on shell
λ_m	$L/m\pi$
ξ	Defined in text
σ	Standard deviation
τ	Time shift for auto-correlation or cross-correlation functions
$\bar{\tau}$	Time corresponding to maximum value of cross-correlation function
ϕ	Radial modal deflection

Ψ_{mn}	Phase angle
Ω	Reduced frequency
ω	Frequency in radians per seconds

Subscripts and Superscripts

A	Indicates relationship to area
a,b	Indicate response points a and b, respectively
F	Indicates relationship to generalized force
I,J	Indicate modes I and J, respectively
k,l	Indicate sub-areas k and l, respectively
N	Indicates normalized function
p,q,w	Indicates relationship to pressure, normal coordinate, and deflection, respectively

Matrix Notation

$[\ ]$	Square matrix
$\lfloor\ \rfloor$	Row matrix
$\lfloor\ \rfloor^T$	Transpose of row matrix
$\left\{\ \right\}$	Column matrix

Note: Double subscripts or superscripts appearing on symbols within a matrix imply all possible combinations of themselves as they vary from unity to their maximums. As the subscripts or superscripts vary, they give the row and column designation within the matrix; the first subscript or superscript gives the row, and the second gives the column. Thus, the variability of the subscripts or superscripts is limited by the number of rows and columns in the matrix.

Miscellaneous Notation

*	Denotes complex conjugate
( )	Parenthesis following a symbol indicates that the symbol is a function of those variables appearing within the parenthesis

$\langle\ \rangle$	Indicates a time average

Differentiation of a variable with respect to time is indicated by dots over the variable.

AERODYNAMICS

Probably the most perplexing area of investigation inherent with the determination of the response is the aerodynamic representation of the fluctuating pressures acting on the structure. Some research has been conducted in the theoretical aspects of the turbulent flow field with as yet few practical results. A promising approach toward understanding the phenomenon occurring in a turbulent boundary layer is the wave guide model for turbulent shear flow as developed by Landahl (Reference 4) as part of this study. The basic formulation of this model is that the turbulent fluctuations in a boundary layer may be represented mathematically by a superposition of shear waves of random phase and orientation in which the mean shear flow acts as a wave guide. The stability characteristics of a turbulent boundary layer velocity profile and the relation of such to the statistics of the pressure fluctuations are consequently investigated. Although, admittedly, this report is just an initial step in the complex problem of turbulence, there is hope that further development might lead to better understanding of the turbulence problem.

Since there exists at this time no "clean" mathematical representation of the fluctuating pressures inherent in buffeting flows, the response analysis developed herein is based on the use of experimentally obtained aerodynamic data. These data may be determined either by wind tunnel testing or in-flight measurements. With the increased emphasis on space-vehicles, a wealth of wind tunnel test data is being obtained for many spacecraft configurations. References 7 - 11 are typical compilations of reduced wind tunnel data of various scaled spacecraft-booster configurations. These include typical power spectra, cross-spectra, auto-correlations and cross-correlations. Realistically, the present state-of-the-art in the aerodynamics representation dictates the use of appropriate spectral data reduction of experimentally measured fluctuating pressures for determining the input data to be used in the response studies. It is seldom practical to obtain sufficient data to provide complete input information; consequently, the experimental data will generally be used to fit analytic expressions for extrapolation purposes.

The fluctuating pressure data are used in response computations in either of two ways, depending on the assumptions made when deriving the response equations. For both cases, the shell surface is divided into many small sub-areas (Figure 1) for computational purposes. One method of handling the pressure data is to assume that the measured pressure at the center of a sub-area is representative of the pressure field at all points within that sub-area. The correlation between any two points in different sub-areas is assumed to equal the correlation between the centers of the two sub-areas. This is henceforth classified as the constant correlation assumption. A pressure power spectrum is required for each sub-area and a pressure co-spectrum (real part of the cross-spectrum) is needed for every pair of sub-areas. This information may be determined by standard data reduction techniques such as those used to obtain the data given in References 7 - 11. This assumption is plausible provided that it is feasible to divide the total surface into sufficiently small

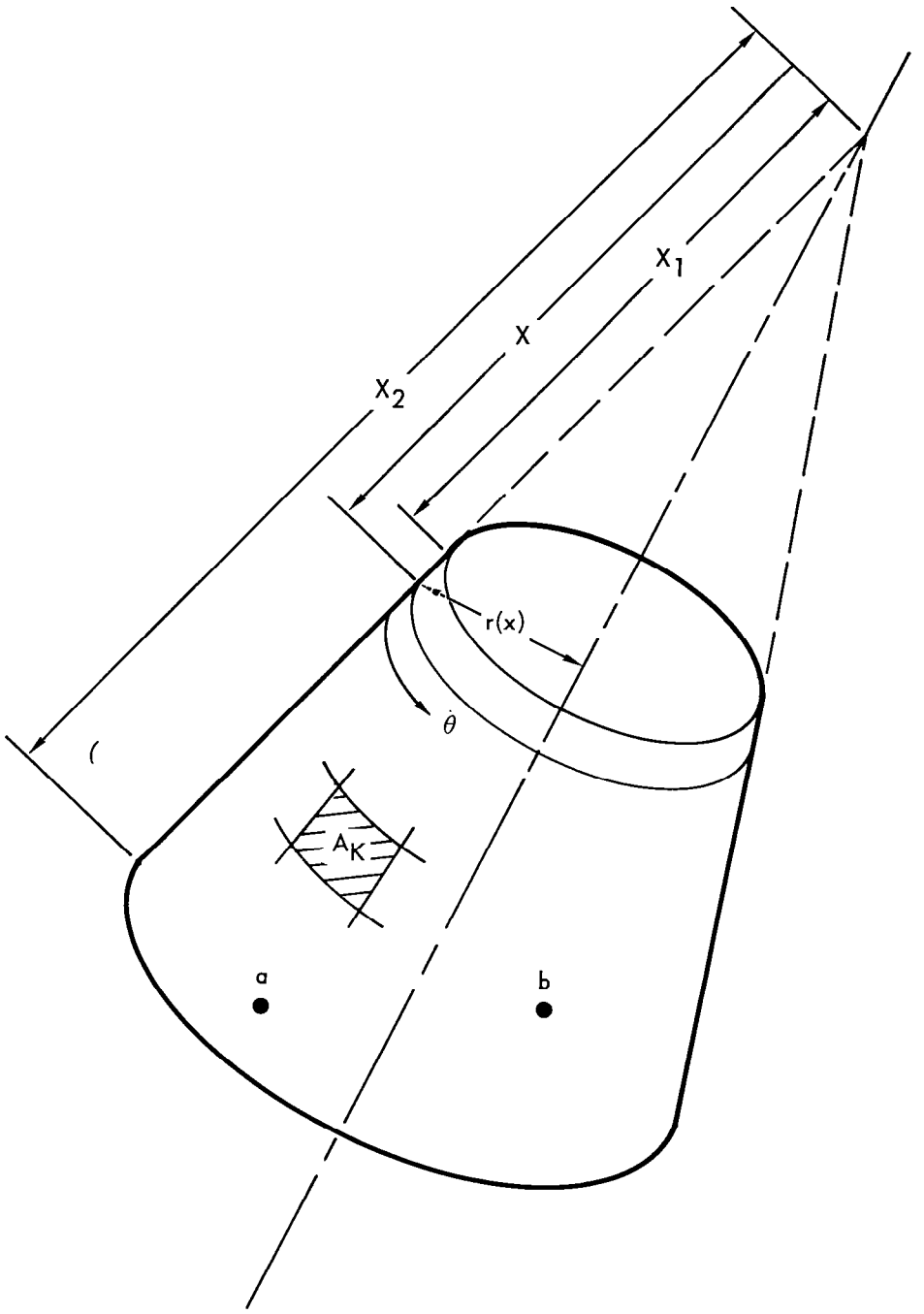

Figure 1 – Coordinate System for Truncated Conical Shell

sub-areas. For the cases examined in this study division into sufficiently small areas was not practical. Therefore, a second fluctuating pressure idealization was employed as covered in the following paragraphs.

Instead of assuming a homogeneous pressure distribution of each sub-area, a more realistic model of the pressure disturbances is utilized. When the pressure fluctuations are generated by a protrusion or by an abrupt change in contour, a simple convective flow pattern is established. This is modeled as a simple decaying convected flow pattern in which the spatial decay rates are determined from experimentally obtained cross-correlations between transducer pairs in both the streamwise and circumferential directions. A continuous pressure distribution over the entire surface is established which may be integrated over each sub-area to improve on the constant correlation assumption. This approach is given detailed treatment later.

Typical streamwise decay rates are given in Figure 2 which is taken

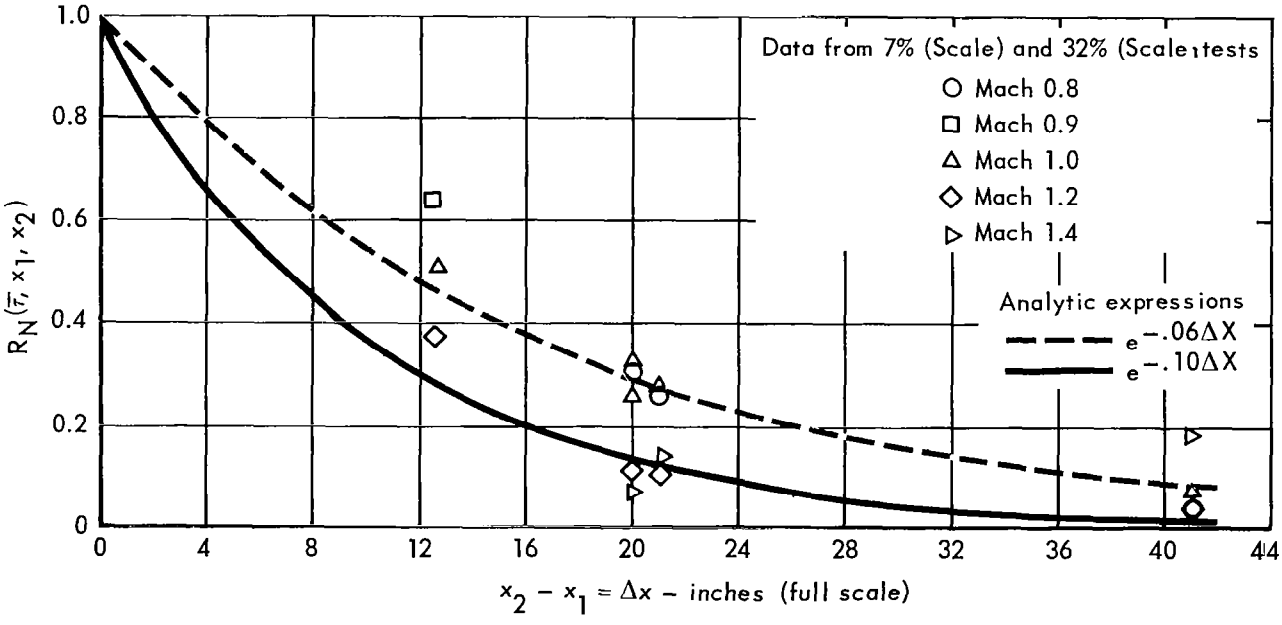

Figure 2— Streamwise Pressure Correlation — Mercury/Atlas Adapter

from the data of References 7 and 8. The normalized cross-correlation of two pressures at x_1 and x_2, $R_N(\bar{\tau}, x_1, x_2)$, is obtained from

$$R_N(\bar{\tau}, x_1, x_2) = R_{max}(\bar{\tau}, x_1, x_2) / \sqrt{R(0, x_1)\, R(0, x_2)} \qquad (1)$$

where $R(0,x_1)$ and $R(0,x_2)$ are the auto-correlations for $\tau = 0$, and $R_{MAX}(\bar{\tau},x_1,x_2)$ is the maximum value of the un-normalized cross-correlation function occurring when $\tau = \bar{\tau}$. The correlation of the pressures between streamwise transducer pairs on the Mercury/Atlas adapter showed that the use of an exponential spatial decay, $e^{-\alpha\Delta x}$, is reasonable. The analytical curves for $e^{-\alpha\Delta x}$ for two values of α are given for illustrative purposes. It is of interest to note that the decay rate appears to increase with increasing Mach number. The circumferential decay rate data, $e^{-\beta r\Delta\theta}$, is similarly given in Figure 3. The actual decay rates used in subsequent response computations were extrapolated from Figures 2 and 3 in a manner discussed later.

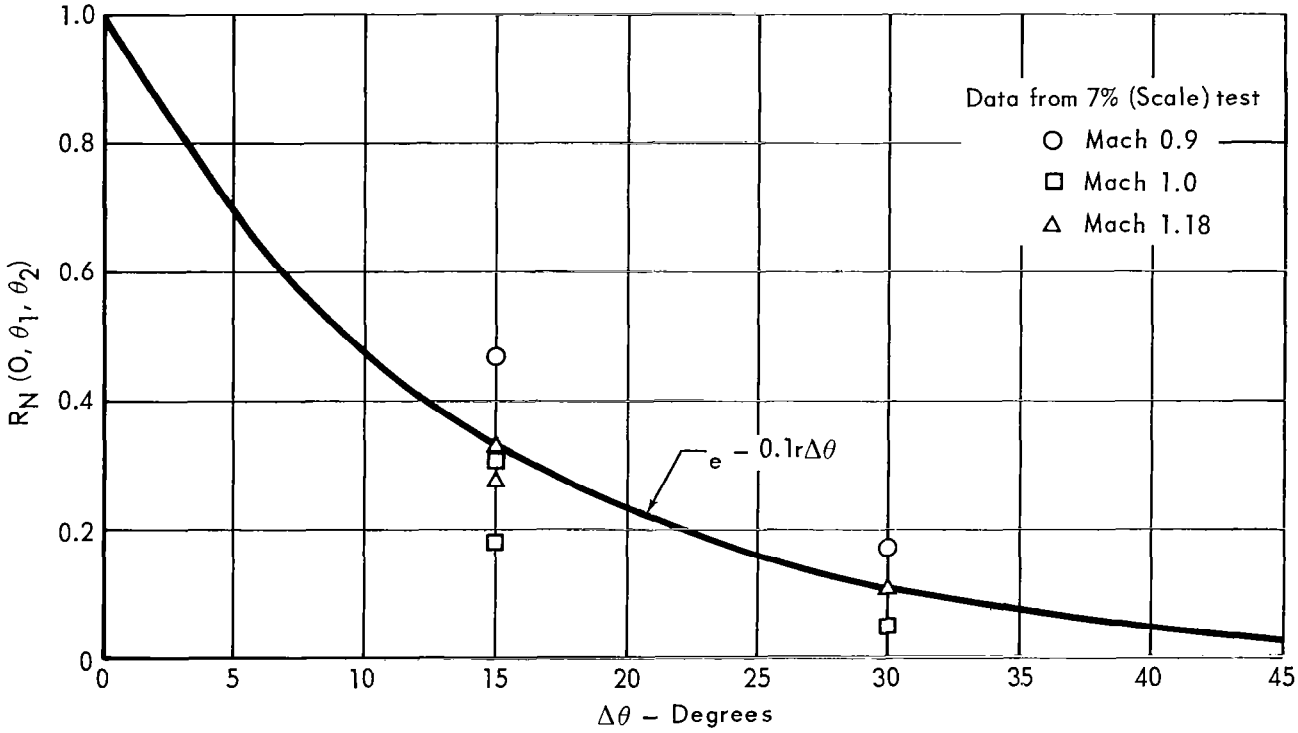

Figure 3 – Circumferential Pressure Correlation–Mercury/Atlas Adapter

The degree of excitation depends on the velocity at which the decaying pattern is convected, as well as the streamwise and circumferential decay rates. The convection velocity may be determined by the relation $U_c = \Delta x/\bar{\tau}$, where $\bar{\tau}$ is the time shift at which the cross-correlation function is a maximum and Δx is the separation between points x_1 and x_2. A value of $U_c = 0.4\ U_\infty$ was used for the work herein, although this is a lower value than associated with a well developed aerodynamic boundary layer, experimental investigations have shown reduced values of convection velocity associated with flows generated by a protrusion or cone-cylinder intersection.

In regard to the aerodynamic excitation of a structure, the effect of vehicle angle of attack on the pressure input parameters has been considered. An option exists in the response program to allow input of different pressure levels for each sub-area of the structure (total of 112). However, it has been discovered that small angles of attack have negligible effect on the pressure input for the nearly cylindrical adapter sections behind conical shapes like the Mercury capsule. A comparison of the power spectra and normalized co-spectra (References 7, 8 and 10) showed small effect due to small variations in angle of attack. Of course, for precise response calculations, it would be desirable to have wind tunnel data at all of the actual flight conditions; however, from the standpoint of cost and time, this is usually not feasible. It is felt that available wind tunnel data on a given configuration can be used with reasonable expectation that the final response calculations will be insensitive to small variations in angle of attack.

An attempt was made to relate the fluctuating pressures, Δp_{rms}, on the configuration surface to the total drag of the body (Reference 13). However, since Δp_{rms} is a characteristic value of a particular point on the vehicle surface while the total drag is an integrated quantity of pressure and shear forces over its surface, the drag can only supply information on an over-all basis. Depending on local conditions, protuberances, sharp corners, shock wave interactions, cavities, etc., the actual pressure fluctuations in the vicinity of such points and at points downstream from these may be considerably different from the mean level. Thus, at the present, the prediction of the actual fluctuating pressures at such points and their downstream influence is still a matter of crude engineering judgement and relies exclusively on direct experimental methods.

Other fluctuating pressure data have become available since Reference 13 was published and analysis of these data suggests the feasiblity of correlating fluctuating pressure levels on various configurations. Compilations of fluctuating pressure data from the Mercury/Atlas and Saturn/Apollo configurations (Reference 12) has revealed several interesting preliminary trends.

One of the trends indicated in Reference 12 is illustrated in Figure 4 which shows the variation of $\Delta C_{p_{rms}}$ with Mach number for the Mercury/Atlas configuration. In general, the fluctuating pressure level decreases with increasing Mach number above 1.0. This was also true for other configurations.

Another result of this compilation of fluctuating pressure data is the statistical distribution of all $\Delta C_{p_{rms}}$ data. An example of the probability distribution of the pressure levels is shown in Figure 5 which gives the distributions separately for the two configurations and also for the combined total. All $\Delta C_{p_{rms}}$ data were plotted irrespective of Mach number, transducer location, and angle of attack. Superimposed upon this figure for reference are three Rayleigh distribution curves for which the analytical distribution is given by

$$\text{Prob}\ (\Delta C_{p_{rms}}/\sigma) = (\Delta C_{p_{rms}}/\sigma) e^{-(\Delta C_{p_{rms}})^2/2\sigma^2} \qquad (2)$$

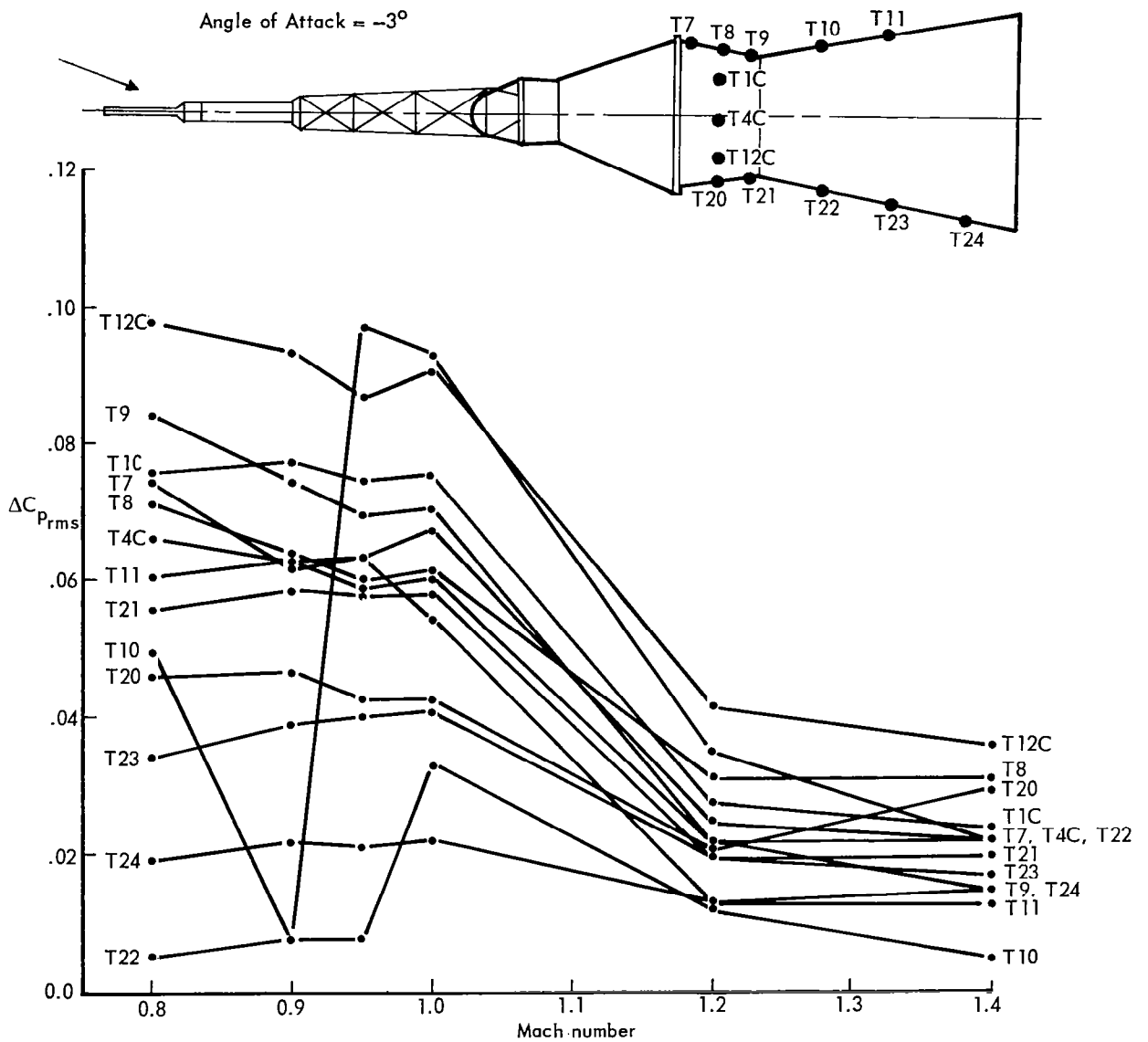

Figure 4 – Fluctuating Pressure Coefficients for Mercury/Atlas – Escape Configuration

where σ is the standard deviation. This type of curve can yield valuable information for preliminary design purposes. An explanation of the use of random process theory and application to physical problems is given in Reference 14.

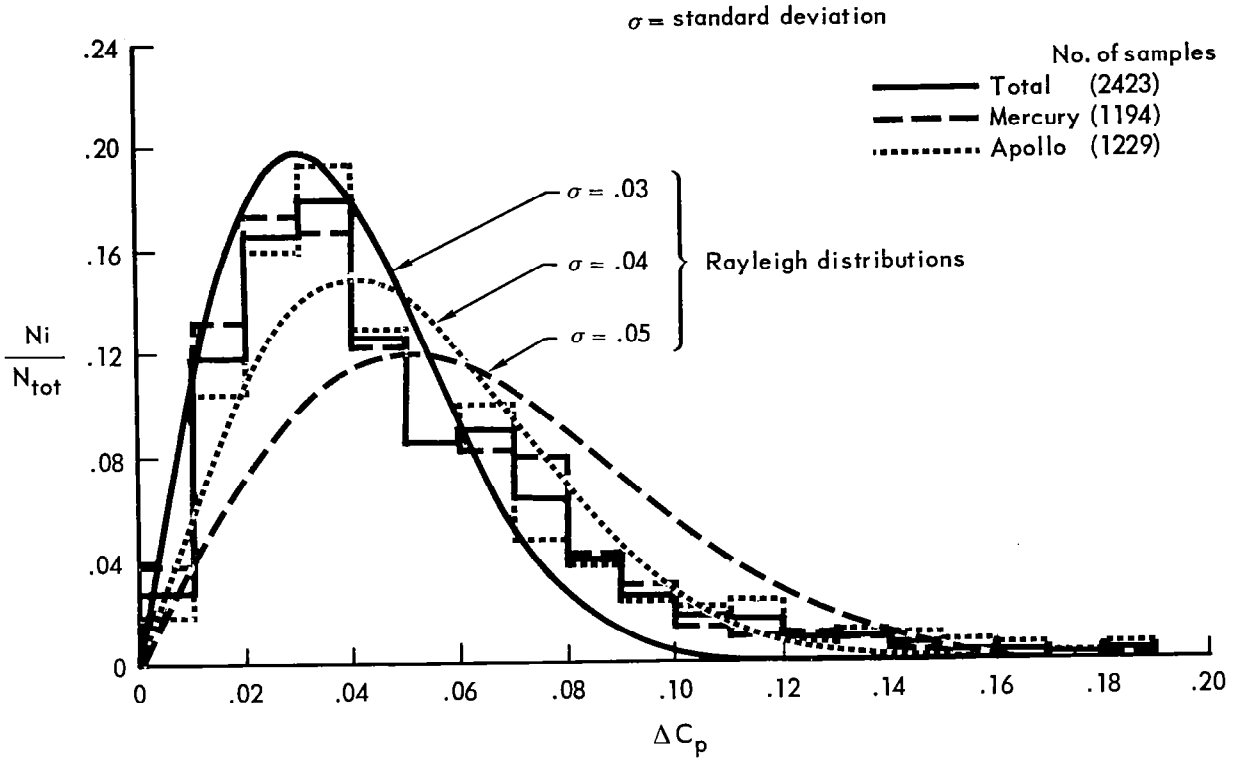

Figure 5 – Probability Density of Composite ΔC_{prms} Data

STRUCTURAL VIBRATION CHARACTERISTICS

With the complexities inherent in the geometry of spacecraft structures (rings, stiffeners, concentrated packages, etc.), most analytical representations of the natural vibration characteristics for a component structure are extremely complicated. For these complex structures, any detailed theoretical shell vibration analysis entails a great amount of time, labor and computer facilities. However, valuable insight on the vibration characteristics of certain systems can be obtained from relevant published work. In many cases, for preliminary shell response calculations, the structure can be idealized such that rough estimates of mode shapes and frequencies can be obtained.

The analytical representation of the dynamics of the Mercury/Atlas adapter used in the present studies was based on a Rayleigh energy method adapted for an axisymmetric ring-stiffened conical shell, Reference 15. The assumed deformation shapes for the conical shell displacements u, v, and w (Figure 6) are:

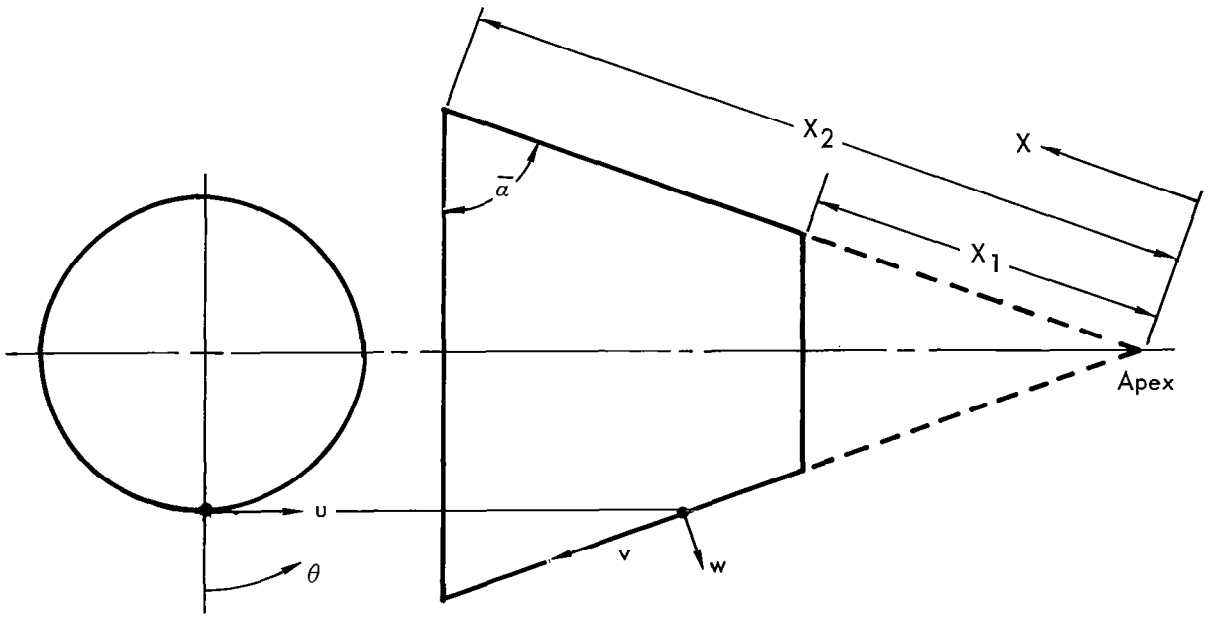

Figure 6 – Coordinate System Employed for Conical Shell Vibration Studies.

$$w = A_m^n[x \cos \bar{\alpha} \sin \frac{x-x_1}{\lambda_m} \cos n\theta][\cos(\omega_{mn} t - \psi_{mn})] \quad (3)$$

$$u = B_m^n[x \cos \bar{\alpha} \sin \frac{x-x_1}{\lambda_m} \sin n\theta][\cos(\omega_{mn} t - \psi_{mn})] \quad (4)$$

$$v = C_m^n[x \cos \bar{\alpha} \cos \frac{x-x_1}{\lambda_m} \sin n\theta][\cos(\omega_{mn} t - \psi_{mn})] \quad (5)$$

where $\lambda_m = L/m\pi$, with m the number of longitudinal half-waves, n the number of circumferential waves, and L the length of the shell frustum along a generator. A_m^n, B_m^n, and C_m^n are the generalized coordinates for each mode (m,n).

The above theoretical analysis was modified to account for the reduction of stiffness due to warping of the stiffener flanges. This modification seems justified since the actual structure consisted of thin deep flanges which are susceptible to warping. The inclusion of the warping modification reduced the lowest analytical frequency (n = 2, m = 1) from 215 cps to 172 cps, which is in better agreement with the experimental frequency as determined from ground vibration tests. For the Mercury/Atlas adapter, the natural frequency spectrum so calculated is shown in Figure 7 along with corresponding measured experimental data. A similar analysis was conducted on this configuration in Reference 16 by idealizing the shell as a cylinder.

To allow for arbitrary circumferential orientation of the ring modes, a complementary set of modes should be included which incorporate the complementary trigonometric functions of θ in Equations (3), (4), and (5). These complementary modes have been included in the response program when the orientation of the modes is arbitrary. When the orientation of the modes is fixed in some manner, say by a very heavy mass attached to the shell, these additional modes are unnecessary. This phenomena has been discussed in References 13 and 17.

In many cases, this form of analysis is insufficient to adequately represent the vibration characteristics of the shell, especially with heavy equipment attached to the shell. In this case, there usually exists completely "distorted" mode shapes which cannot be represented by a single sine or cosine mode number. Elaborate structural analysis is then required such as presented in Reference 18.

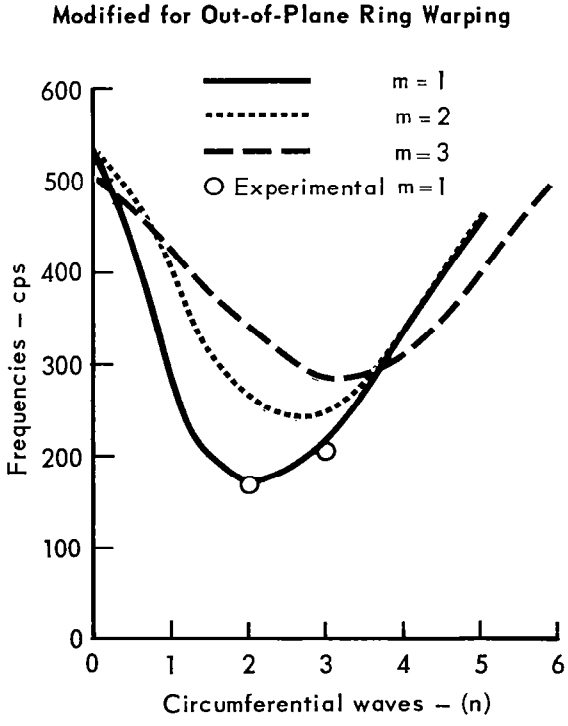

Figure 7 – Mercury/Atlas Adapter–Natural Frequency Spectrum

Even with sufficient analytical tools at hand, the complex systems encountered in the space industry are usually not amendable to treatment by theoretical methods. Consequently, one must resort to experimentally determined vibration characteristics. Three methods are available to fulfill experimental evaluation of a particular shell structure: (1) dynamically scaled model tests, (2) full-scale tests, and (3) component matching techniques. The actual selection of any method is dictated by factors such as cost, time, available facilities, complexity of structure, etc. Each method has advantages and disadvantages which must be considered. Although dynamically scaled models are valuable, or even necessary in some cases, the model expense and scaling problems usually eliminate this method for obtaining adequate vibration data on localized sections such as adapters. Sound ground vibration testing techniques on prototype structures would give the most beneficial and complete data. The Gemini/Titan adapter was tested in this manner with mode shapes, frequencies, generalized masses, and damping ratios determined for 14 modes. It was found that much care was required to separate certain closely spaced modes. Reference 19 summarizes the methods and results of these tests. The component matching technique (Reference 20) appears to be feasible for determining vibration characteristics for assembled structures. This method in general can be used if data is obtained on integral parts of the system before final assembly.

In spite of the numerous methods of obtaining vibration characteristics of shells (analytical and/or experimental), the final input of vibration data to be used for determining the response of a particular configuration must be based on sound engineering judgment. With this in mind, the response program to be discussed subsequently has been developed with two options available for the input of vibration data: (1) the use of theoretical analysis based on Equations (3) through (5) including complementary modes, and (2) a Fourier series representation which allows incorporation of mode shapes other than the simple trigometric functions. This latter option is handled by synthesizing the mode shapes determined experimentally or by more complex analysis by Fourier series representation (Reference 6). The pertinent vibration data required by the response program is the number of modes (maximum of 25), mode numbers (n,m) if first option is employed or Fourier coefficients for the second option, and corresponding generalized masses and damping ratios for each mode.

The concept of damping is in itself a complex problem, with the usual solution to the problem being that of simply assuming small damping (1%). However, in determining the response, the magnitude of peak-response at resonant frequencies is inversely proportional to the damping ratio (ζ) used in the calculations; consequently, sound experinced judgment, or reliable test data should be used. In the vibration of complex structures, so many interactions occur that an adequate representation of the damping ratio is difficult. As discussed in Reference 21 localized damping at structural joints is not only influenced by the material and configuration, but also by the firmness or tightness of the connection, and also by the mode of vibration. In the ground vibration tests of the Gemini/Titan configuration,

damping values of 1% to 5% were determined. In the comparison of the flight and calculated response studies made on the Mercury/Atlas adapter, an average of the available damping ratios, $\zeta = .02$, was determined from the limited decay data taken on this configuration (Reference 23).

RESPONSE ANALYSIS

General Discussion

Reference 5 gives a detailed analysis of the response of shell-type structures to random pressure excitation. The derivation is slanted toward structures represented as truncated conical shells, which includes the idealization of a moderately tapered spacecraft adapter. This analysis results in equations for the deflection and acceleration response co-spectra or as special cases, the response power spectra which are more generally of interest in determining structural adequacy. In the discussion that follows, the pertinent equations derived in Reference 5 will be given along with the assumptions necessary to derive them.

Development of Response Equations

Up to this point, it has not been specified which response power spectrum is to be determined; i.e., which coordinate response, u, v, or w, is desired. Since the method of calculating any of these coordinate responses is identical, it is arbitrary whether one or all are obtained. Because the only measured data available is for the radial coordinate w, it has been chosen as the coordinate for which the response equations are developed.

Assuming the shell indicated in Figure 1 is lightly damped with radial coordinate normal modes $\phi_I(x,\theta)$, corresponding to a set of normal coordinates q_I, the radial shell response at any point a to pressure excitation $p(x,\theta,t)$ is given by:

$$w(x_a,\theta_a,t) = [\phi_{aI}]\{q_I(t)\} \tag{6}$$

$$\ddot{q}_I(t) + 2\zeta_I\omega_I\dot{q}(t) + \omega_I^2 q_I(t) = \frac{1}{M_I}\int_{x_1}^{x_2}\int_0^{2\pi}\phi(x,\theta)p(x,\theta,t)r(x)d\theta dx \tag{7}$$

The assumption of light damping allows one to neglect cross damping terms in the above equation.

The excitation pressure of interest here is that due to a turbulent aerodynamic flow field. Consequently, $p(x,\theta,t)$ is random in nature which requires that Equations (6) and (7) be solved in terms of statistical averages. With the assumption of an ergodic random process (a discussion of what this involves is given in Reference 5), equivalent statistical

averages may be obtained from either time averages over infinite extent or ensemble averages. Because $p(x,\theta,t)$ is available only as a function of time, it is necessary to use time averages. One of the requirements of an ergodic process is that it be stationary; with this assumption the response cross-spectrum between any two points a and b (see Figure 1) can be related to the Fourier transforms of the response as follows:

$$S_w^{ab}(\pm\omega) = \lim_{T\to\infty} \frac{1}{2T} \int_{-T}^{T} e^{-i\omega t} w(x_a,\theta_a,t)\,dt \int_{-T}^{T} e^{i\omega t} w(x_b,\theta_b,t)\,dt \tag{8}$$

The notation $\pm\omega$ is used to indicate that the cross-spectrum defined by Equation (8) covers both the positive and negative frequency ranges. In practice, $w(x_a,\theta_a,t)$ and $w(x_b,\theta_b,t)$ are usually truncated such that they equal zero for $t \geq T$, where T is a long time. Then Equation (8) can be written as:

$$S_w^{ab}(\pm\omega) = \frac{1}{2T} w(x_a,\theta_a,\pm\omega)\; w^*(x_b,\theta_b,\pm\omega) \tag{9}$$

where

$$w(x_a,\theta_a,\pm\omega) = \int_{-\infty}^{\infty} e^{-i\omega t}\; w(x_a,\theta_a,t)\,dt \tag{10}$$

$$w^*(x_b,\theta_b,\pm\omega) = \int_{-\infty}^{\infty} e^{i\omega t}\; w(x_b,\theta_b,t)\,dt \tag{11}$$

It is not actually necessary to make the truncation assumption at this time, although to do so allows a more direct and simpler mathematical derivation, and pre-recognizes the fact that a similar assumption concerning the pressure excitation $p(x,\theta,t)$ would be necessary later. In other words, it is recognized that the final equations must ultimately depend upon the excitation $p(x,\theta,t)$ which can only be determined for finite time.

Substitution of Equations (6) and (7) into Equation (8) and after considerable manipulation, the following equation results for the deflection response cross-spectrum.

$$S_w^{ab}(\pm\omega) = [\phi_{aI}][S_q^{IJ}(\pm\omega)][\phi_{bJ}]^T \tag{12}$$

$$S_q^{IJ}(\pm\omega) = \frac{1}{Z_I(\pm\omega)Z_J^*(\pm\omega)} \int_{x_1}^{x_2}\int_{0}^{2\pi}\int_{x_1}^{x_2}\int_{0}^{2\pi} \Big(S_p(x,\theta,x',\theta',\pm\omega)\phi_I(x,\theta)\phi_J(x',\theta') \; r(x)r(x')\,d\theta\,dx\,d\theta'\,dx' \Big) \tag{13}$$

where

$$Z_I(\pm\omega) = M_I\omega_I^2\left(1 - \left(\frac{\omega}{\omega_I}\right)^2 + i2\zeta_I\left(\frac{\omega}{\omega_I}\right)\right) \tag{14}$$

$$Z_J^*(\pm\omega) = M_J\omega_J{}^2\left(1 - \left(\frac{\omega}{\omega_J}\right)^2 - i2\zeta_J\left(\frac{\omega}{\omega_J}\right)\right) \tag{15}$$

The quantities Z_I and Z_J^* above are reciprocals of the complex frequency response function for modes I and J, respectively. The primes in Equation (13) are to indicate the order of integration.

Equation (13) gives the normal coordinate cross-spectrum between any two normal coordinates q_I and q_J. As first pointed out by Powell (Reference 23) these cross-spectra represent the statistical dependence between normal coordinate responses. When I and J are equal, Equation (13) gives a normal coordinate response power spectrum.

The function $S_p(x,\theta,x',\theta',\pm\omega)$ is the pressure cross-spectrum between any two points (x,θ) and (x',θ') on the shell surface. It is given by a relationship similar to Equation (9), i.e.,

$$S_p(x,\theta,x',\theta',\pm\omega) = \frac{1}{2T}\,p(x,\theta,\pm\omega)p^*(x',\theta',\pm\omega)$$

but is more fundamentally defined as the Fourier transform of the pressure cross-correlation function, $R_p(x,\theta,x',\theta',\tau)$. This correlation function is given by:

$$R_p(x,\theta,x',\theta',\tau) = \lim_{T\to\infty}\frac{1}{2T}\int_{-T}^{T} p(x,\theta,t+\tau)p(x',\theta',t)\,dt \tag{16}$$

Thus,

$$S_p(x,\theta,x',\theta',\pm\omega) = \int_{-\infty}^{\infty} e^{-i\omega\tau} R_p(x,\theta,x',\theta',\tau)\,d\tau \tag{17}$$

Response Equations With Constant Correlation Assumption

The analytical definition of $S_p(x,\theta,x',\theta',\pm\omega)$ over the complete shell surface is impractical either theoretically or empirically when the exciting pressure results from a highly turbulent boundary layer. Yet this is precisely the condition under which maximum excitation of spacecraft shell-type structures occur. Reference 5 attempts to resolve this dilemma by dividing the total shell surface into many sub-areas and assuming a different homogeneous pressure acting over each sub-area with appropriate correlation of pressures between sub-areas. This is referred to as the constant correlation assumption in Reference 5. By subdividing the shell, Equation (13) can be written as

$$S_q^{IJ}(\pm\omega) = \frac{1}{Z_I(\pm\omega)Z_J^*(\pm\omega)} \sum_k \sum_l \int_{A_l} \int_{A_k} \Big(S_p(x,\theta,x',\theta',\pm\omega)\phi_I(x,\theta)\phi_J(x',\theta') \; r(x)r(x')\,d\theta\,dx\,d\theta'\,dx' \Big) \tag{18}$$

where $\int_{A_k}$ and $\int_{A_l}$ indicate integrations over the individual sub-areas. Then by the constant correlation assumption, Equation (18) can be simplified as follows:

$$S_q^{IJ}(\pm\omega) = \frac{1}{Z_I(\pm\omega)Z_J^*(\pm\omega)} \sum_k \sum_l S_p^{kl}(\pm\omega) \left(\int_{A_k} \phi_I(x,\theta)r(x)\,d\theta\,dx \; \int_{A_l} \phi_J(x',\theta')r(x')\,d\theta'\,dx' \right) \tag{19}$$

In essence, this assumption implies that $S_p^{kl}(\pm\omega)$ is independent of the precise surface location of the spatial coordinates within the areas A_k and A_l. When $l = k$, $S_p^{kk}(\pm\omega)$ is the power spectrum of the pressure on A_k. When $l \neq k$, $S_p^{kl}(\pm\omega)$ is the cross-spectrum of the pressures acting on A_k and A_l, assumed to be represented by the pressures acting at the area centers.

Equation (19) can be written in terms of matrix algebra as:

$$S_q^{IJ}(\pm\omega) = \frac{1}{Z_I(\pm\omega)Z_J^*(\pm\omega)} \lfloor \phi_{Ik}^A \rfloor [S_p^{kl}(\pm\omega)] \lfloor \phi_{Jl}^A \rfloor^T \tag{20}$$

where

$$\phi_{Ik}^A = \int_{A_k} \phi_I(x,\theta)r(x)\,d\theta\,dx \tag{21}$$

$$\phi_{Jl}^A = \int_{A_l} \phi_J(x',\theta')r(x')\,d\theta'\,dx' \tag{22}$$

Equations (12) and (20) give the deflection response cross-spectrum for points a and b. This cross-spectrum has both a real and imaginary part, the real part being the response co-spectrum and the imaginary part being the response quad-spectrum. When b = a in the equations, the response power spectrum at point a results. For this condition, the imaginary part is

identically zero since a power spectrum by definition has no imaginary part. The work of Reference 5 continues from Equation (20) by eliminating the imaginary part and subsequently writing equations for the response co-spectrum which are limited to the positive frequency domain in cycles per second. Since the primary interest herein is the response power spectrum, these equations are written below for the special case of b = a.

$$C_w^{aa}(f) = \lfloor \phi_{aI} \rfloor [C_q^{IJ}(f)] \lfloor \phi_{aJ} \rfloor^T \tag{23}$$

$$C_q^{IJ}(f) = \frac{(1/M_I M_J \omega_I^2 \omega_J^2) G(f) \lfloor \phi_{Ik}^A \rfloor [C_p^{kl}(f)] \lfloor \phi_{Jl}^A \rfloor^T}{G^2(f) + H^2(f)}$$

$$+ \frac{(1/M_I M_J \omega_I^2 \omega_J^2) H(f) \lfloor \phi_{Ik}^A \rfloor [Q_p^{kl}(f)] \lfloor \phi_{Jl}^A \rfloor^T}{G^2(f) + H^2(f)} \tag{24}$$

where

$$G(f) = \left(1 - \left(\frac{f}{f_I}\right)^2\right)\left(1 - \left(\frac{f}{f_J}\right)^2\right) + 4\zeta_I \zeta_J \frac{f^2}{f_I f_J} \tag{25}$$

$$H(f) = 2\zeta_J \frac{f}{f_J}\left(1 - \left(\frac{f}{f_I}\right)^2\right) - 2\zeta_I \frac{f}{f_I}\left(1 - \left(\frac{f}{f_J}\right)^2\right) \tag{26}$$

The normal coordinate co-spectrum, $C_q^{IJ}(f)$, is the real part of Equation (24). The elements of $[C_p^{kl}(f)]$ and $[Q_p^{kl}(f)]$ entering into Equation (24) are given by the real and imaginary parts, respectively, of Equation (17) when that equation is written as a function of f for the pressures acting at the center of areas A_k and A_l. That is,

$$C_p^{kl}(f) = \int_{-\infty}^{\infty} \cos(2\pi f\tau)\, R_p^{kl}(\tau) d\tau \tag{27}$$

$$Q_p^{kl}(f) = \int_{-\infty}^{\infty} \sin(2\pi f\tau)\, R_p^{kl}(\tau) d\tau \tag{28}$$

with $R_p^{kl}(\tau)$ given by

$$R_p^{kl}(\tau) = \lim_{T \to \infty} \frac{1}{2T} \int_{-T}^{T} p_k(t+\tau) p_l(t) dt \tag{29}$$

Equations (23) through (29) can be solved directly for the deflection response power spectrum at a, but to do so requires a considerable amount of computation for shell-type structures. This results from the need to include a large number of normal modes and many sub-areas for such shell structures. As pointed out in Reference 5, this computation can be reduced by the reciprocal of the number of modes if the contributions of Equation (24) are neglected except when $J = I$, i.e., if the normal coordinate co-spectra are neglected.

In Reference 5, a general criterion is developed for determining the maximum possible contribution of a normal coordinate co-spectrum. The criterion indicates that this contribution decreases with decreased modal damping and with increased frequency separation of the normal modes. Thus, it is possible to neglect most of the normal coordinate co-spectra due to the relatively large frequency separation of the modes. Generally, however, for shell-type structures, some modes have small separation frequencies. To investigate this problem, two response calculations were made, one neglecting the normal coordinate co-spectra, i.e., when $I \neq J$, and the other including them. This response study used theoretical sine-cosine modes and fluctuating pressure data determined from wind tunnel tests. In all, nineteen modes were used with many of them very closely spaced (for example, 277 and 280 cps, and 336 and 337 cps). Even so, the maximum percentage error incurred by neglecting the normal coordinate co-spectra, was 15 percent in the magnitude of the spectra at any frequency, and 3% based on rms levels. **While this response study cannot be considered general, it is felt to be typical** for a shell subjected to buffeting flows excitation. Thus, it appears to be **justifiable to neglect the normal coordinate co-spectra ($I \neq J$) for the problem under study. This is especially true when one considers the other uncertainties involved, such as use of model wind tunnel aerodynamic data as representative of inflight excitation and the complexities of determining an adequate structural representation of shells, including structural damping.**

With the elimination of the normal coordinate co-spectra, Equations (23) and (24) become

$$C_w^{aa}(f) = \sum_I \phi_{aI}^2 \, C_q^{II}(f) \tag{30}$$

$$C_q^{II}(f) = \frac{\left[\phi_{Ik}^A\right]\left[C_p^{kl}(f)\right]\left[\phi_{Jl}^A\right]^T}{M_I^2 \, \omega_I^4 \left[\left(1 - \left(\frac{f}{f_I}\right)^2\right)^2 + \left(2\zeta\left(\frac{f}{f_I}\right)\right)^2\right]} \tag{31}$$

The acceleration response power spectra are given in terms of the above by:

$$C_{\ddot{w}}^{aa}(f) = \sum_I \phi_{aI}^2 \, C_{\ddot{q}}^{II}(f) \tag{32}$$

$$C_{\ddot{q}}^{II}(f) = (2\pi)^4 f^4 C_q^{II}(f) \tag{33}$$

The associated mean-square responses are given by the integrals of Equations (30) through (33), i.e.,

$$\langle w^2(x_a,\theta_a,t)\rangle = \int_0^\infty C_w^{aa}(f)df \tag{34}$$

$$\langle q_I^2(t)\rangle = \int_0^\infty C_q^{II}(f)df \tag{35}$$

$$\langle \ddot{w}^2(x_a,\theta_a,t)\rangle = \int_0^\infty C_{\ddot{w}}^{aa}(f)df \tag{36}$$

$$\langle \ddot{q}_I^2(t)\rangle = \int_0^\infty C_{\ddot{q}}^{II}(f)df \tag{37}$$

Equations (30) through (37) along with Equations (27) and (29) give the pertinent response power spectra and the associated mean-square responses when the constant correlation assumption is utilized. Such an assumption would be justified if the sub-areas selected for this representation were small relative to the spatial scale of the buffeting pressures. However, for the cases considered in this study, it has been found that this assumption was not valid.

Response Equations With Integrated Pressure Correlation

As discussed in Reference 13, the calculated response spectra of the Mercury/Atlas Adapter yielded highly conservative results when compared to actual flight measurements if the input pressure was assumed completely correlated over each sub-area A_k into which the adapter was divided, Figure 1. Some discrepancy is expected due to the assumptions used in the development of the response equations, in addition to the unknown loading conditions applied on the flight vehicle, such as induced bending moments, axial forces, etc. However, the predominant reason for any discrepancy is due to the constant correlation assumption which implies that the measured pressures at given locations represent a homogeneous pressure field over the entire sub-area surrounding this point. Since the response program (Reference 6) is limited to a maximum division of the shell surface into 112 areas, the corresponding area sizes could have significant influence on the calculation results. The calculated generalized force for each area (employing the constant correlation assumption) is

$$S_F^{kk}(\omega) = S_p(\omega) \left[\int_{A_K} \phi_I \, dA_k\right]^2 \qquad (38)$$

where $S_p(\omega)$ is the power spectrum of the homogeneous pressure over each area. With a convected pressure field acting over the shell, Equation (38) can be overly conservative if the size of the area A_k is significant. Therefore, investigations have been made to determine a practical and reasonable modification which may be applied to the response formulation to account for the convected pressure field.

The parameters which would effect the generalized force acting on each area are the characteristics of the flow field, the structural mode shapes and the area dimensions. Theoretically, the exact method of calculating the cross-spectrum contribution of a pair of areas to the generalized force is of the following form,

$$S_F^{kl}(\omega) = \int_{A_l}\int_{A_k} S_p\,(x,\theta,x',\theta',\omega)\ \phi_I(x,\theta)\phi_I(x',\theta')\ dA_k dA_l \qquad (39)$$

where $\phi_I(x,\theta)$ and $\phi_I(x',\theta')$ represent the ith mode shape over the respective surface coordinates x,θ and x',θ'. $S_p(x,\theta,x',\theta',\omega)$ is the cross-spectrum of the random pressure field.

When $A_k = A_l$ then $S_F^{kk}(\omega)$ represents the spectral density of the generalized force acting on a given area A_k. If the power spectra $S_p^{kk}(\omega)$ and $S_p^{ll}(\omega)$ of the pressures at representative points within the areas A_k and A_l are used as a reference and if only the co-spectrum of generalized force (real part of Equation (39)) is retained, Equation (39) can be written as:

$$C_F^{kl}(\omega) = \sqrt{S_p^{kk}(\omega)S_p^{ll}(\omega)}\int_{A_l}\int_{A_k} C_N(x,\theta,x',\theta',\omega)\phi_I(x,\theta)\phi_I(x',\theta')dA_k dA_l \qquad (40)$$

where $C_N(x,x',\theta,\theta',\omega)$ is the normalized co-spectra defining the pressure field. Equation (40) is the familiar form for the determination of the joint acceptance of the ith mode (References 17 and 24).

Although theoretically the form of the generalized force as given in Equation (40) should be incorporated in any analysis to modify response calculations based on a homogeneous pressure over an area, circumstances such as core capacity limitations of the IBM 7094 imposed on the response program necessitated a simpler method. Consequently an average mode approach has been developed which assumes that the generalized force co-spectrum for a pair of areas is given by

$$C_F^{kl}(\omega) = \sqrt{S_p^{kk}(\omega)S_p^{ll}(\omega)} \cdot \frac{\int\phi_I dA_k \int\phi_I dA_l}{A_k A_l} \int_{A_l}\int_{A_k} C_N(x,\theta,x',\theta',\omega)dA_k dA_l \qquad (41)$$

where $\int\phi_I dA_k$ is the integral of the ith mode shape over area A_k.

Since the modification employed as an option in the response program is of the form given in Equation (41), comparisons between Equations (40) and (41) are presented in Appendix A for a simple structure (simply-supported panel) to show the confidence that can be realized in the average mode (approximate) approach.

The evaluation of the equations necessitates a description of the correlation function of the pressure field and the modal representation of the structure, $\phi_I(x,\theta)$. For a turbulent fluctuating pressure field the decay between two streamwise points is a function of time τ and separation distance ξ. Consequently, as a first order approximation, the total streamwise decay can be represented by independent functions of time τ and separation distance ξ as

$$D \simeq e^{-\mu\tau}\, e^{-\alpha\xi} \tag{42}$$

where μ and α are decay coefficients. Similarly by assuming the lateral decay is only a function of space (independent of time), the decay can be represented by $e^{-\beta\eta}$ where β is a decay coefficient and η is the lateral separation. The cross-correlation function of pressure between two points separated spatially by distances ξ and η (always positive) can be approximated by

$$R_p(\xi,\eta,\tau) = R_o(\tau-\tau')\, e^{-\alpha\xi} e^{-\beta\eta} \tag{43}$$

where $R_o(\tau-\tau')$ represents an auto-correlation function shifted by τ'. Now with the definition of the cross-power spectrum given as

$$S_p(\xi,\eta,\omega) = \lim_{T\to\infty} \frac{1}{2T} \int_{-T}^{+T} e^{-i\omega\tau} R(\xi,\eta,\tau)\, d\tau \tag{44}$$

and by substituting Equation (43), and integrating, the real part (co-spectrum) of the power spectra is

$$C_p(\xi,\eta,\omega) = S_p(\omega) C_N(\xi,\eta,\omega) = S_p(\omega)\, e^{-\alpha\xi}\, e^{-\beta\eta} \cos\Omega \tag{45}$$

where $\Omega = \frac{\omega\xi}{U_c}$, $C_N(\xi,\eta,\omega)$ is the normalized co-spectra

and U_c = convection velocity = ξ/τ'.

Thus, by substituting $C_N(\xi,\eta,\omega)$ as defined in Equation (45) into Equation (41), one obtains the co-spectrum of generalized force for areas A_k and A_l. By summing the resulting equation over k and l, where the indices take on all values from unity to the maximum number of areas, there results the power spectrum of the total generalized force for mode I.

With this in mind the normal coordinate response power spectra C_q^{II} is given as

$$C_q^{II}(f)=\frac{\sum_k \sum_l \int_{A_k}\phi_I(x,\theta)dA_k \cdot \int_{A_l}\phi_I(x',\theta')dA_l \cdot \sqrt{S_p^{kk}(f)\, S_p^{ll}(f)}\int_{A_l}\int_{A_k} C_N(\xi,\eta,f)dA_k dA_l}{A_k A_l M_I^2 \omega_I^4\left[\left(1-(\frac{f}{f_I})^2\right)^2+\left(2\zeta_I(\frac{f}{f_I})\right)^2\right]} \tag{46}$$

where the frequency variable has been changed from ω to f to agree with Equation (31). Thus when using the integrated pressure correlation, the above equation is used in place of Equation (31) for determining the shell response.

COMPARISON OF CALCULATED AND FLIGHT ACCELERATION SPECTRA

Having derived the fundamental response equations, the accuracy of this analyses can only be illuminated by actual comparisons between calculated response and measured flight data. With flight acceleration data of the Mercury/Atlas adapter available from the MA-4 flight, comparisons at six Mach numbers were made. All calculated response studies were made with the best possible simulation of the actual flight vehicle and aerodynamic environment consistent with the capability of the IBM 7094 computer. Using the response program (Reference 6), the acceleration spectra and mean-squared response were determined for the frequency range of 0-600 cps.

The vibration data incorporated were determined from analytical results modified to match the lower ground vibration test frequencies on the actual flight configuration of the Mercury/Atlas adapter. The number of modes used was 19. Table I presents the necessary vibration characteristics. With very limited damping taken on the ground vibration tests, an estimate of the damping ratio had to be incorporated for all modes. A damping ratio of .02 measured in lower modes was used throughout the analysis. Admittedly, this is a gross assumption, but comparisons made with subsequent Gemini/Titan adapter ground vibration test results indicate that this value of damping may be reasonable.

To adequately represent the aerodynamic excitation input, one must resort to fluctuating pressure data obtained on the configuration in question from controlled wind tunnel tests. However, in some cases, even this information is not available (or reliable) and then one must draw on his resourcefulness in assembling available data to estimate the pressure levels and correlations that would exist on the configuration to be analyzed. For the response calculations on the Mercury/Atlas adapter, three sources of aerodynamic data were available.

TABLE I
VIBRATION CHARACTERISTICS MERCURY/ARLAS ADAPTER
Damping Ratio = .02 (All Modes)

Mode No. Circum. n	Mode No. Long. m	Generalized Mass Lb-Sec^2/In	Frequency (cps)
2	1	90.34	172
3	1	83.08	215
3	2	78.60	248
2	2	79.74	277
3	3	66.60	280
1	1	109.24	288
4	3	66.85	313
4	1	80.57	336
4	2	77.69	337
2	3	66.02	348
5	3	67.07	406
1	2	78.29	415
1	3	64.96	438
5	2	77.67	464
5	1	80.29	469
6	3	67.56	507
0	3	64.31	508
0	1	77.95	529
0	2	73.77	532

There were two wind tunnel tests run on scaled configurations: (1) 7% scale, and (2) 32% scale. The reduced pressure data for the 7% scale test is presented in Reference 7 and for the 32% scale tests, References 8 and 10. The third source consisted of limited flight data on the pressure levels from the series of Mercury/Atlas flights. Coe (Reference 25) illuminates the fact that the fluctuating pressure levels from the 32% scale tests are in general considerably higher (especially around Mach 1.0) than the flight data. Comparison of the 7% scale wind tunnel pressure data with flight data shows these data to be more representative of the inflight pressure levels. Consequently, these data were used for the response calculations. Statistically reduced pressure data were available at 3 Mach numbers: 0.9, 1.0, and 1.18, for this purpose.

To provide greater Mach number coverage the limited data discussed above was extrapolated to Mach numbers of 0.6, 1.5, and 2.0. The power spectra of the pressure at these Mach numbers were determined from scaling relations based on convected homogeneous turbulence. This relationship is based on the fact that the mean-squared pressure is given by:

$$\langle p^2 \rangle = \int_0^\infty S_p(f)\,df \tag{47}$$

and the reduced frequency is

$$\Omega = \frac{fD}{U_\infty} \tag{48}$$

where D is a characteristic length of the model. Therefore, the relationship between $\Delta C_{p_{rms}}$ and the pressure power spectra is

$$\frac{U_\infty}{q_d^2 D} \int_0^\infty S_p(\Omega) d\Omega = \frac{\langle p^2 \rangle}{q_d^2} = \Delta C_{p_{rms}}^2 \tag{49}$$

If it is assumed that the power spectra has approximately the same distribution with dimensionless frequency at all Mach numbers, then the level of the power spectra can be determined by the relationship

$$S_p(\Omega)_2 = k\, S_p(\Omega)_1 \tag{50}$$

where the subscripts indicate different Mach numbers and

$$k = \left(\frac{q_{d_2}}{q_{d_1}}\right)^2 \left(\frac{(\Delta C_{p_{rms}})_2}{(\Delta C_{p_{rms}})_1}\right)^2 \left(\frac{U_{\infty_1}}{U_{\infty_2}}\right)$$

Likewise, the frequencies are scaled according to

$$\left(\frac{fD}{U_\infty}\right)_1 = \left(\frac{fD}{U_\infty}\right)_2 \tag{51}$$

Consequently, using Equations (50) and (51) as the scaling criteria, the response calculations at Mach 0.6, 1.5, and 2.0 were run using as reference the pressure levels at Mach 1.18 (7% scale). The pressure power spectra were scaled with the aid of the dashed curve shown in Figure 8. The points shown in Figure 8 are average values of $\Delta C_{p_{rms}}$ determined from the collation of fluctuating pressure data of wind tunnel tests on the Mercury/Atlas configuration (Reference 12). All data used for scaling pressure input are given in Table II.

For all response studies, the adapter was divided into 80 sub-areas, 4 streamwise and 20 circumferentially, with the average size of each area being 12.7 inches x 11 inches. The Form I expansion (Figure 9) was used in the analysis which required as input the pressure power-spectrum for each area in a strip, and the normalized co-spectrum between all areas within the two strips. The modification to account for the pressure variations over each area was incorporated in the calculations. If normalized co-spectrum data were not available from wind tunnel tests, these terms were calculated from Equation (B4) in Appendix B.

TABLE II

AERODYNAMIC INPUT DATA - MERCURY/ATLAS ADAPTER

Mach No.	Pressure Data	ΔP_{rms} $\frac{Lb}{ft^2}$	Dynamic Pressure q_d-Lb/Ft^2	$\Delta C_{P_{rms}}$	Scale Factors* Pressure	Scale Factors* Frequency	Convection Velocity U_C-Ft/Sec	Decay Rates - 1/in. α	Decay Rates - 1/in. β
0.60	Extrapolated	17.50	350	.050	.720	.51	235	.030	.050
0.90	7% Scale	37.05	570	.065	----	---	370	.036	.070
1.00	7% Scale	40.30	650	.062	----	---	410	.053	.126
1.18	7% Scale	28.49	770	.037	1.00	1.00	470	.077	.118
1.50	Extrapolated	21.60	900	.024	.354	1.31	618	.090	.100
2.00	Extrapolated	18.53	975	.019	.135	1.75	820	.100	.100

*The scale factors were obtained from Equations (50) and (51) using as reference the 7% Scale Wind Tunnel data at M = 1.18.

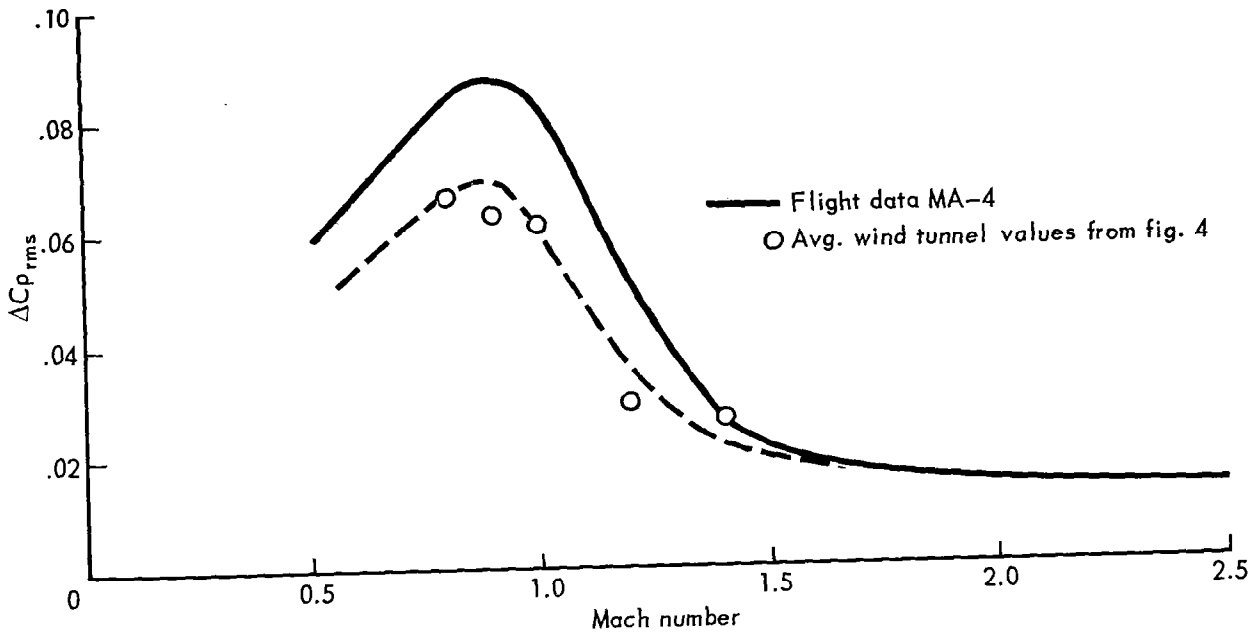

Figure 8 – Fluctuating Pressure Coefficients, Mercury/Atlas Adapter

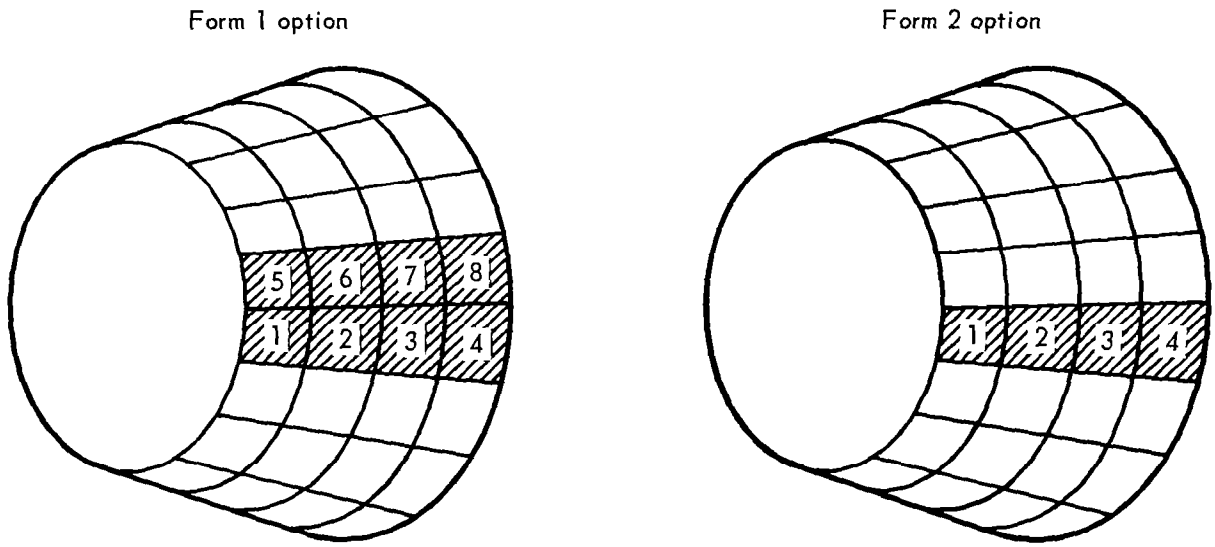

Figure 9 – Correlation Areas Used in Response Computer Program

The response program was used to determine the acceleration response at an adapter station at which flight data were available. The actual in-flight (MA-4) values of g's rms, Figure 10, were obtained from Reference 26 for the frequency band of 0-600 cps. The calculated rms values for the same frequency band are shown for comparison. The comparison of the overall levels for the six Mach numbers at which the response was calculated is surprisingly good, probably better than should be expected for such a complex problem. The calculated response at Mach numbers 0.6, 1.5, and 2.0 were obtained by scaling the pressure power spectra (Mach 1.18) using Equations (50) and (51). The results indicate that this scaling technique is valid in lieu of measured pressure data especially since the trend of the calculated rms values follows the actual flight data very well.

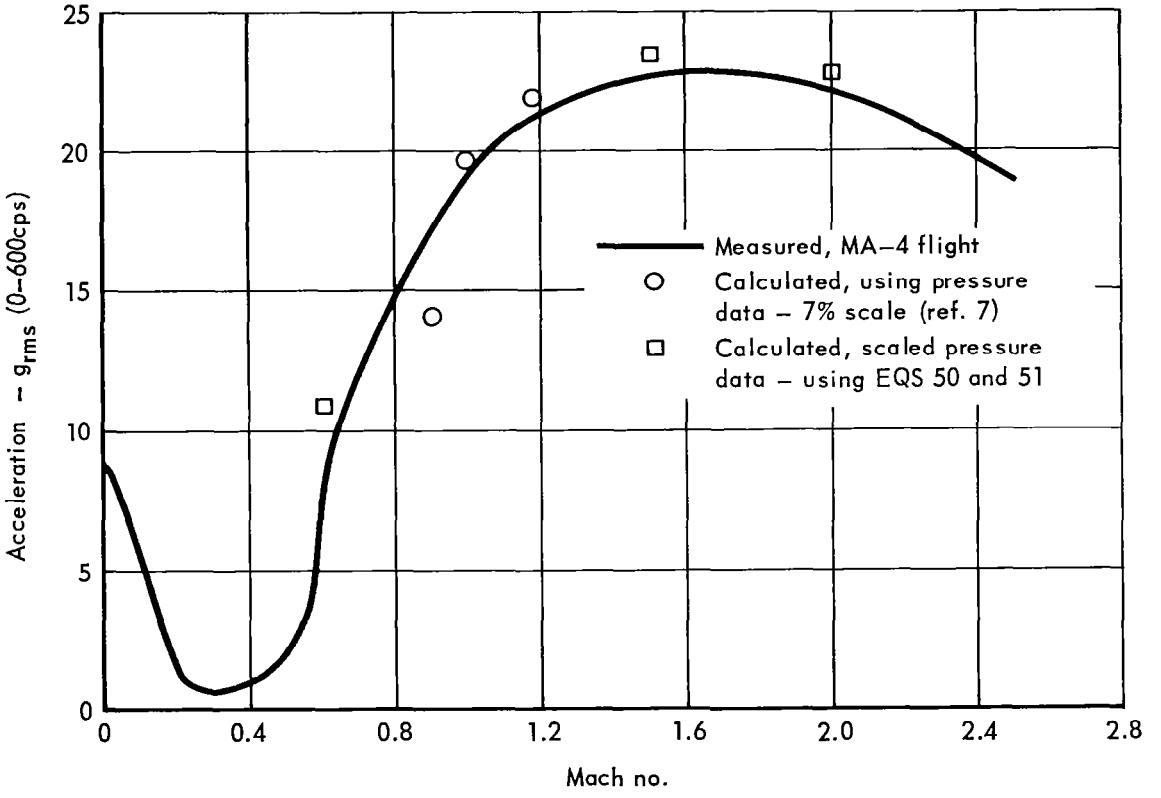

Figure 10 – Comparison of rms Acceleration – Measured and Calculated

If the input, $\Delta C_{p_{rms}}$, and the output, g_{rms}, is plotted versus Mach number as shown in Figure 11, it is seen that the pressure at Mach 2.0 is twice as effective in producing response as that at Mach 1.0.

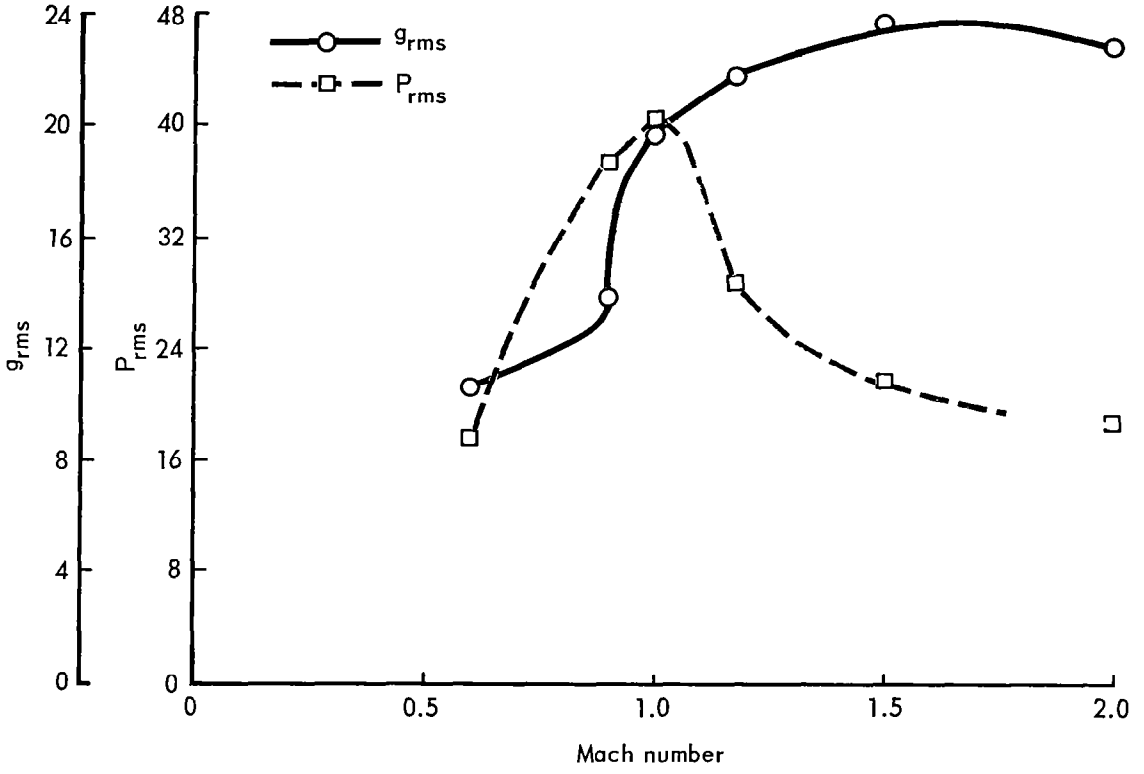

Figure 11 – rms Pressure and Acceleration vs Mach Number

The comparison of the acceleration power spectrum 0-600 cps at Mach 1.0 (7% scale pressure data) is shown in Figure 12, and the comparison at Mach 2.0, using extrapolated pressure data, is shown in Figure 13. These were typical of the other runs in that the order of magnitude of the peaks are compatible with the flight response although there exists a shifting of the spectra. This frequency shifting might be expected based on the premise that the modified analytical vibration data which were used in the response studies could be significantly different than the inflight vibration characteristics. However, unpublished experimental data of the Mercury/Atlas configuration have shown that the in-plane loading (axial compression and bending) has no significant effect on the vibration characteristics. Other factors which might affect the vibration of the structure are steady-state aerodynamics, temperature, and pressure differential. Although these conditions would affect, in some degree, the response of the vehicle, the variation of particular configurations and flight trajectories will usually circumvent

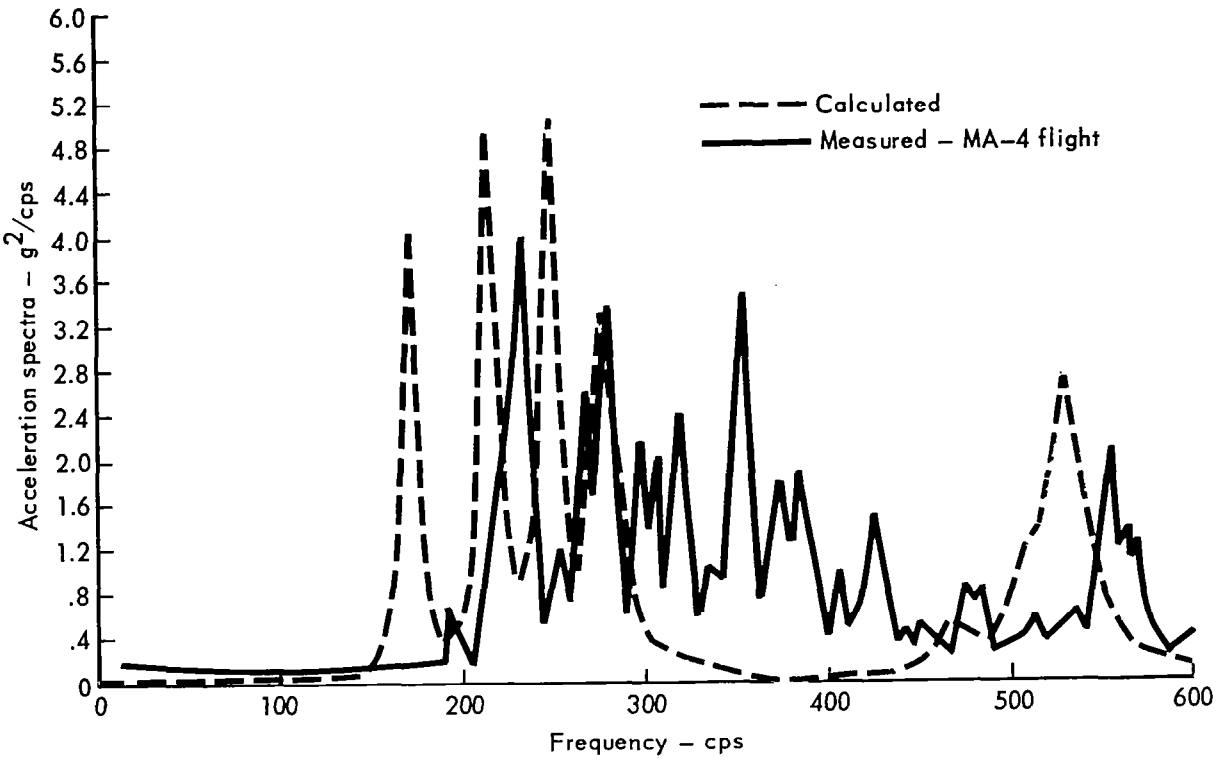

Figure 12 – Measured and Calculated Acceleration Spectra at Mach 1.0 – Mercury/Atlas Adapter

adequate representation of such loading for response predictions. With the results obtained from these response comparison studies, it is felt the over-all response characteristics can be obtained if adequate aerodynamic input is available for a particular configuration.

Concluding Remarks

The principal development of this research is a method of predicting the response of complex shells to fluctuating pressure. This has resulted in a computer program for calculating the acceleration and/or deflection response spectra at discrete locations on the shell. The computation scheme requires as input either analytical or experimental vibration data, and fluctuating pressure power spectra and co-spectra data from wind tunnel tests supplemented by empirically derived analytical expressions. Although the present response analysis has been based on the use of experimentally obtained aerodynamic data, an analytical study of a wave guide model for turbulent shear flow has been initiated and with further development gives hope that the fundamental mechanism will be understood.

Comparison studies were made between measured inflight data and calculated acceleration response of the Mercury/Atlas adapter for Mach numbers

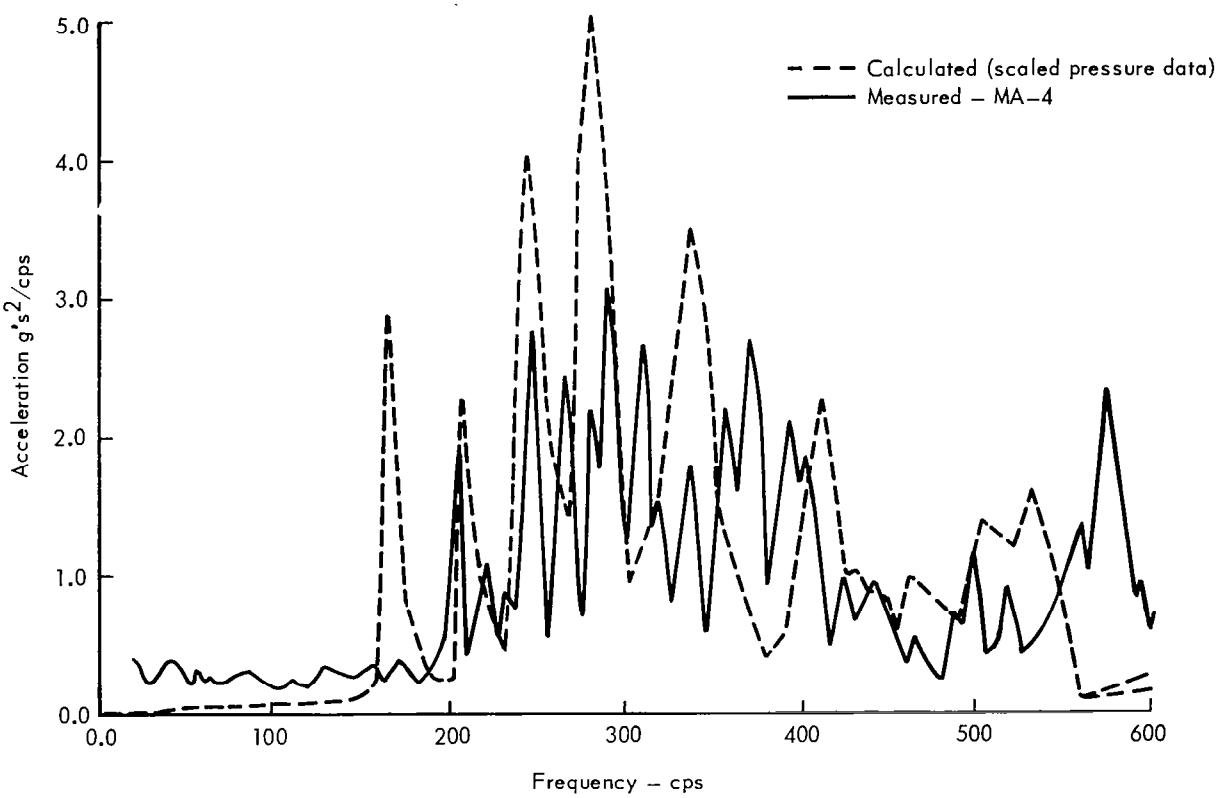

Figure 13 – Measured and Calculated Acceleration at Mach 2.0 – Mercury/Atlas Adapter

0.6 to 2.0. It was found that rms acceleration levels can be predicted although the individual spectral distribution might not be in agreement at some frequencies. If good vibration data and wind tunnel pressure data are available, it is felt that the computed shell response will provide an adequate estimate of the actual flight vehicle response to buffeting flows.

APPENDIX A

COMPARISON OF THE AVERAGE AND EXACT CORRELATION METHODS

The development of the shell response equations has included a modification to the constant correlation assumption which accounts for the convected pressure field over each sub-area, A_k, of the shell structure. The total decay of the pressure is assumed to be represented by independent functions of time τ, streamwise separation distance ξ, and lateral separation η. With this assumption, the normalized co-spectrum can be written

$$C_N(\xi,\eta,\omega) = e^{-\alpha\xi}\, e^{-\beta\eta} \cos\frac{\omega\xi}{U_c} \tag{A1}$$

To correctly account for this form of the pressure field, the generalized force equation should be of the form

$$C_F^{k\ell}(\omega) = \sqrt{S_p^{kk}(\omega)S_p^{\ell\ell}(\omega)} \int_{A_\ell}\int_{A_k} C_N(x, y, x', y', \omega)\, \phi_I(x, y)\phi_I(x', y')dA_k\, dA_\ell \tag{A2}$$

where $S_p^{kk}(\omega)$ and $S_p^{\ell\ell}(\omega)$ are the homogeneous power spectra for areas A_k and A_ℓ, respectively. However, due to limitations of core storage of the computer, Equation (A2) was simplified by assuming an average mode approach such that only the normalized co-spectrum is integrated over each sub-area which results in

$$C_F^{k\ell}(\omega) = \sqrt{S_p^{kk}(\omega)S_p^{\ell\ell}(\omega)}\, \frac{\int\phi_I\, dA_k \int\phi_I\, dA_\ell}{A_k\, A_\ell} \int_{A_\ell}\int_{A_k} C_N(x, y, x', y', \omega)\, dA_k\, dA_\ell \tag{A3}$$

Therefore, from Equations (A2) and (A3) a frequency dependent modification factor $E^{kk}(\omega)$ for each method can be determined which relates the generalized force and generalized homogeneous pressure for an area A_k by

$$S_F^{kk}(\omega) = S_p^{kk}(\omega)\, A_K^2\, E^{kk}(\omega) \tag{A4}$$

To illuminate the differences of these two methods, a comparison study was made for a simply-supported panel, Figure A1, in which the mode shape can be represented by

$$\phi(x, y) = \sin\frac{m\pi x}{a} \sin\frac{n\pi y}{b} \tag{A5}$$

where a, b are the panel dimensions in the x, y directions, respectively, and m, n are the corresponding mode numbers. Therefore, the integration of Equation (A2) using Equations (A1) and (A5) yields the modification factor for the exact method, which is

$$E_{Ex}^{kk}(\omega) = \left[\frac{C}{(A^2+B^2)^2}\right. \left\{-\phi Z_1+(\frac{m\pi}{a}\xi)^2 Z_2+(\phi Z_3-(\frac{m\pi}{a}\xi)^2 Z_4)\cosh\alpha\xi\cos\Omega \right. \tag{A6}$$

$$+2\alpha\xi\frac{m\pi\xi}{a}Z_5\sinh\alpha\xi\cos\Omega-2\alpha\xi\Omega Z_3\sinh\alpha\xi\sin\Omega$$

$$\left.-2\Omega\frac{m\pi\xi}{a}Z_5\cosh\alpha\xi\sin\Omega\right\} - \frac{D}{(A^2+B^2)^2}\left\{2\alpha\xi\Omega Z_1\right.$$

$$-[\phi Z_3+(\frac{m\pi\xi}{a})Z_4]\sinh\alpha\xi\sin\Omega-2\cosh\alpha\xi\sin\Omega$$

$$(\alpha\xi\frac{m\pi\xi}{a}Z_5)-2\sinh\alpha\xi\cos\Omega[\frac{m\pi\xi}{a}\Omega Z_5]$$

$$\left.\left.-2\alpha\xi\Omega Z_3\cosh\alpha\xi\cos\Omega\right\}\right] x\ \frac{1}{E^2}\left\{(\frac{n\pi\eta}{b})^2 w_1-(\beta\eta)^2 w^2\right.$$

$$\left.+2\cosh\beta\eta[(\beta\eta)^2 w_3-(\frac{n\pi\eta}{b})^2 w_4]+2\beta\eta(\frac{n\pi\eta}{b})w_5\sinh\beta\eta\right\}$$

where $\Omega = \omega\xi/U_c$

$\phi = (\alpha\xi)^2-\Omega^2$

$A = (\alpha\xi)^2+(\frac{m\pi\xi}{a})^2-\Omega^2$

$B = 2\alpha\xi\Omega$

$C = A^2-B^2$

$D = 2AB$

$E = \beta\eta^2+(\frac{n\pi\eta}{b})^2$

$Z_1 = \sin^2(\frac{m\pi X_{u+1}}{a})+\sin^2(\frac{m\pi X_u}{a})$

$Z_2 = \cos^2(\frac{m\pi X_{u+1}}{a})+\cos^2(\frac{m\pi X_u}{a})$

$Z_3 = \cos\frac{m\pi\xi}{a} - \cos\frac{m\pi}{a}(X_{u+1} + X_u)$

$Z_4 = \cos\frac{m\pi}{a}(X_{u+1} + X_u) + \cos\frac{m\pi}{a}\xi$

$Z_5 = \sin\frac{m\pi\xi}{a}$

$w_1 = \cos^2(\frac{n\pi Y_{v+1}}{b})+\cos^2(\frac{n\pi Y_v}{b})$

$w_2 = \sin^2(\frac{n\pi Y_{v+1}}{b})+\sin^2(\frac{n\pi Y_v}{b})$

$w_3 = \sin\frac{n\pi Y_{v+1}}{b}\sin\frac{n\pi Y_v}{b}$

$w_4 = \cos\frac{n\pi Y_{v+1}}{b}\cos\frac{n\pi Y_v}{b}$

$w_5 = \sin\frac{n\pi\eta}{b}$

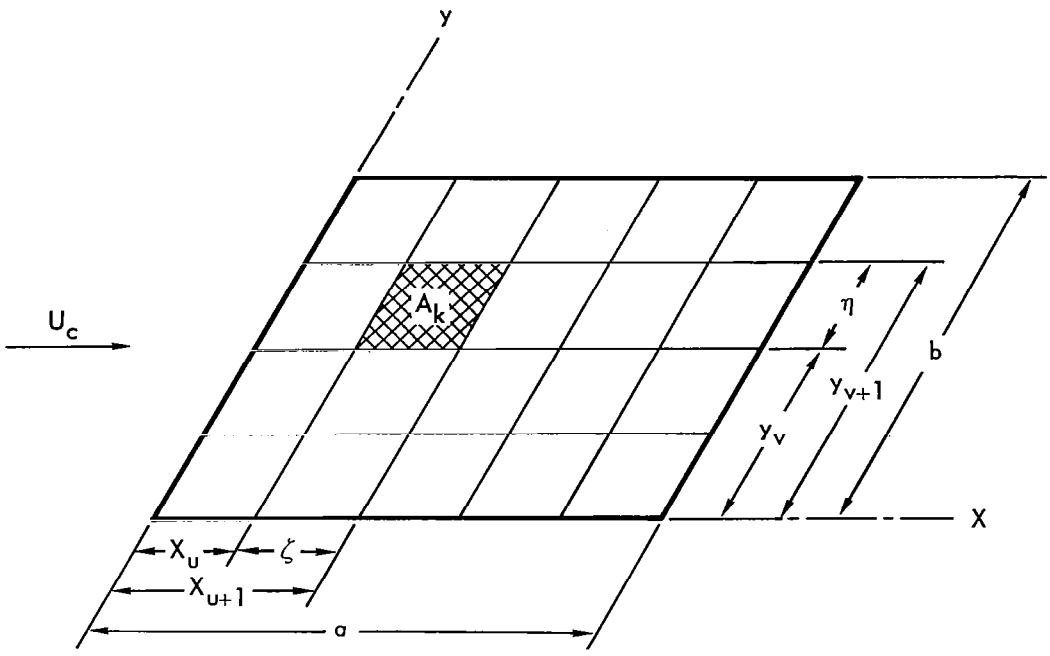

Figure A1 – Panel Configuration for Study of Modification Factors

Likewise, an average mode term is found from integration of Equation (A3),

$$E_{AV}^{kk} = \frac{4K}{[(\alpha\xi)^2+\Omega^2]^2} \frac{(\cosh \beta\eta-1)}{(\beta\eta)^2} \left\{[(\alpha\xi)^2-\Omega^2][\text{Cosh}\alpha\xi\cos\Omega-1]+2\alpha\xi\Omega\sinh\alpha\xi\sin\Omega\right\} \quad (A7)$$

where $K = (\frac{ab}{\xi\eta})^2 \frac{1}{m^2n^2\pi^4} [\cos \frac{m\pi X_{u+1}}{a} - \cos \frac{m\pi X_u}{a}]^2[\cos \frac{n\pi Y_{v+1}}{b} - \cos\frac{n\pi Y_v}{b}]^2$

and $\lim_{\beta\eta \to 0} \frac{\text{Cosh } \beta\eta-1}{(\beta\eta)^2} = \frac{1}{2}$

It was found that for some particular combinations of mode shapes and area locations of the panel the two methods could yield significantly different results. However, although this discrepancy exists for certain sub-areas this, in itself, is meaningless since the overall acceleration or deflection spectra is the quantity that must be compared. The normal coordinate power spectra is given by

$$C_q^{II}(f) = K_I(f)\lfloor \phi_{Ik}^A \rfloor [C_p^{kl}(f)] \lfloor \phi_{I_\ell}^A \rfloor^T \qquad (A8)$$

where $K_I(f) = \dfrac{1}{M_I^2 \omega_I^4 \left\{ [\, 1-(f/f_I)^2]^2 + (2\zeta_I f/f_I)^2 \right\}}$

ϕ_{Ik}^A = integral of the ith mode shape over area A_k

$f = \omega/2\pi$

and from this term the acceleration and/or deflection spectra can be obtained. For any frequency (f) at which Equation (A-8) is calculated $K_I(f)$ will be a constant. Therefore, the investigation of the triple product term will then be the primary area of comparison.

The form of the pressure input for computer purposes is to form a normalized co-spectrum matrix in which the elements of the matrix represent correlations between pairs of areas. The response program (Reference 6) allows two forms of input as shown in Figure 9, in which pressure correlation is assumed over all cross-hatched areas. The Form I expansion assumes pressure correlation over all areas in two adjacent strips, whereas the Form II expansion assumes correlations over all areas in a strip and that these then are representative for all strips in the structure.

To fully develop the comparisons study, a representative panel has been chosen in which the aspect ratio (a/b) is 0.5 and which is divided into 8 equal areas. (See inset in Figure A2.) Since the Form II expansion is to be employed here, elements in the pressure co-spectrum matrix can be computed from the typical strip, for example 1-2 in Figure A2. The normalized co-spectrum matrix (normalized with respect to reference pressure power spectra for the respective sub-areas) for this typical strip is

$$[\Gamma] = \begin{bmatrix} 1 & C_N^{12} \\ C_N^{12} & 1 \end{bmatrix}$$

where C_N^{12} is the normalized pressure co-spectrum between areas 1 and 2 and is representative for all other strips in the structure. The actual pressure levels are then introduced by the triple product $[\Psi][\Gamma][\Psi]$ where

$$[\Psi] = \begin{bmatrix} \sqrt{S_p^{11}(f)} & 0 \\ 0 & \sqrt{S_p^{22}(f)} \end{bmatrix}$$

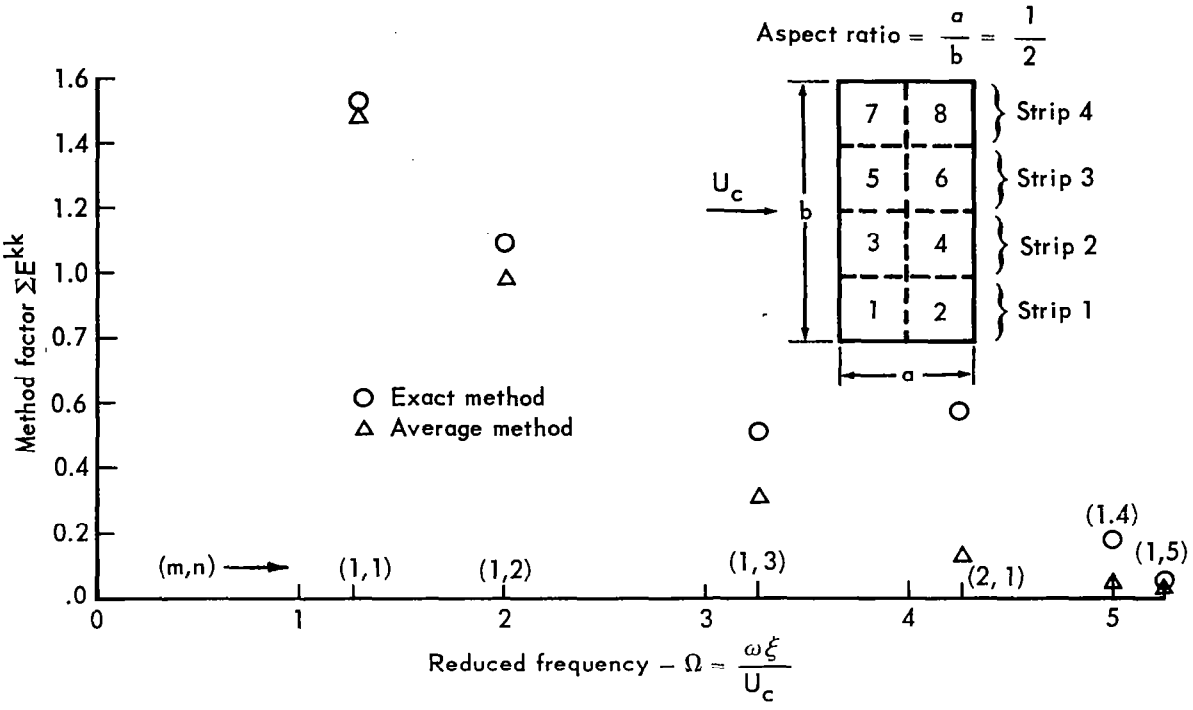

Figure A2 – Comparison of Exact and Average Method Factors.

If for the purposes of comparison and simplicity the normalized co-spectrum terms C_N^{12} are neglected, then Equation (A8) can be written as

$$C_q^{II}(f) = K_I(f) \sum_{k=1}^{n} \left|\phi_{Ik}^A\right|^2 C_p^{kk}(f) = K_I(f) \sum_{k=1}^{n} \left|\phi_{Ik}^A\right|^2 S_p^{kk}(f) \qquad (A9)$$

As stated previously, this equation is based on the assumption that over each area A_k the pressure is perfectly correlated. To correct for the flow field decay over each area, the normalized co-spectrum matrix is modified and consequently for the approximate method, Equation (A9) becomes

$$C_q^{II}(f) = K_I(f) \sum_{k=1}^{n} E_{AV}^{kk}(f) S_p^{kk}(f) A_k^2 \qquad (A10)$$

where E_{AV}^{kk} is defined by Equation (A7) with K representing the ratio $\frac{\left(\int \phi_{Ik} dA_k\right)^2}{A_k^2}$ for the panel.

In a similar manner, the exact form of the modified normal coordinate power spectra can be written as

$$C_{qE}^{II}(f) = K_I(f) \sum_{k=1}^{n} E_{EX}^{kk}(f) S_p^{kk}(f) A_k^2 \qquad (A11)$$

where E_{EX}^{kk} is defined by Equation (A6).

The maximum portion of the total mean-squared response for any frequency bandwidth is contributed from the area at or near the resonance frequencies of the structure. With this in mind comparative values of C_q^{II} as found from Equations (A10) and (A11) were evaluated at frequencies f, and, consequently, reduced frequency Ω, which corresponded to the panel natural frequencies. The frequency equation for a simply-supported panel is

$$\omega_{mn} = \sqrt{\frac{D\pi^4}{\rho h a^4}\left[m^2+n^2r^2\right]} \qquad (A12)$$

where D = plate modulus = $Eh^3/12(1-\nu^2)$

E = modulus of elasticity (psi)

h = thickness of panel

ρ = mass density of panel

r = aspect ratio = a/b

m,n = mode numbers in x,y direction, respectively

and for a given panel, the non-dimensional frequencies at which the normal coordinate power spectra were calculated are given by

$$\omega_{mn}\sqrt{\frac{\rho h a^4}{D\pi^4}} = m^2+n^2r^2. \qquad (A13)$$

Therefore for the panel illustrated in Figure A2 (r = 0.5), the evaluation of $\sum_{k=1}^{8} E^{kk}(f)$ was determined at ratios of Ω dictated by Equation (A13). The comparison as found from this summation would correspond to the evaluation of $C_q^{II}(f)$ if the pressure input $S_p(f)$ was identical for both areas in a strip. Figure A2 shows the comparison of the modification factors for a streamwise decay rate α of 0.05 and a lateral decay rate β of zero where the m,n shown along the abscissa refer to the panel modes which were used in the calculations. The results indicate there exists fair agreement except for the calculation for the 2,1 mode. Additional studies have shown that the discrepancy between the two methods is mainly influenced by the ratio of the streamwise dimension ξ to the structural wave length a/m. In other words it is better to divide the structure surface into sub-areas in which the streamwise length ξ is small in comparison with the smallest structural wave length a/m encountered in the response. Consequently in using the average mode method for modifying the response calculations, it is better to divide the structure into smaller streamwise dimensions ξ at the sacrifice of larger circumferential dimensions η.

APPENDIX B

CALCULATION OF NORMALIZED CO-SPECTRUM TERM

An interesting aspect which results when using the simple convected flow pattern to modify the response equations is that terms inherent in the normalized co-spectrum matrix [Γ], could be calculated in lieu of adequate measured wind tunnel data. As discussed previously, the response equations have been formulated using an average mode approach in which the generalized force co-spectrum between two sub-areas A_k and A_ℓ is given by

$$C_F^{k\ell}(\omega) = -\sqrt{S_p^{kk}(\omega) \quad S_p^{\ell\ell}(\omega)} \; \frac{\int \phi_I \, dA_k \int \phi_I \, dA_\ell}{A_k \; A_\ell} \int_{A_\ell} \int_{A_k} C_N(x, \theta, x; \theta; \omega) \, dA_k dA_\ell \tag{B1}$$

with the normalized pressure co-spectra defined by

$$C_N(\xi, \eta, \omega) = e^{-\alpha\xi} \, e^{-\beta\eta} \cos\Omega \tag{B2}$$

where $\Omega = \frac{\omega\xi}{U_c}$. The terms ξ and η refer to separation distances in the streamwise and circumferential directions, respectively and α, β are the associated spatial decay constants. For computation purposes ξ, η are the area dimensions of each sub-area in which the structure is divided.

To calculate the normal co-ordinate power spectra (Equation (31)), a normalized co-spectra matrix must be input which depends on the form of expansion employed, Figure 9. The terms of the normalized co-spectra matrix can be calculated by

$$C_N^{k\ell}(\omega) = \frac{1}{A_k \; A_\ell} \int_{A_k} \int_{A_\ell} C_N(\xi, \eta, \omega) \, dA_k \; dA_\ell \tag{B3}$$

Upon substitution of Equation (B2) into (B3) and integrating, the normalized co-spectrum between two areas k and ℓ is

$$C_N^{k\ell}(\omega) = \frac{1}{[(\alpha\xi)^2+\Omega^2][(\beta\eta)^2} \left\{ [(\alpha\xi)^2-\Omega^2][e^{-k\alpha\xi}\cos k\,\Omega + \right.$$

$$e^{-(k-2)\alpha\xi}\cos(k-2)\Omega - 2e^{-(k-1)\alpha\xi}\cos(k-1)\Omega]$$

$$\left. + \delta_{k_1}\alpha\xi\Omega(e^{\alpha\xi}-e^{-\alpha\xi})\sin\Omega \right\} \left\{ e^{-\ell\beta\eta} + e^{-(\ell-2)\beta\eta} - 2e^{-(\ell-1)\beta\eta} \right\} \tag{B4}$$

where $\delta_{k_1} = 1.$ if $k = 1.$

$= 0$ if $k \neq 1.$

and the k and ℓ refer to the separation longitudinally (flow direction) and circumferentially of the areas, respectively. Referring to Figure 9 for area notation, then if k = ℓ = 1., $C_N^{k\ell}(\omega)$ becomes the modification factor for any area as given by

$$C_N^{kk}(\omega) = \frac{4}{[(\alpha\xi)^2+\Omega^2]^2} \frac{(\cosh \beta\eta-1)}{(\beta\eta)^2} \left\{[(\alpha\xi)^2-\Omega^2][\cosh \alpha\xi \cos\Omega-1]+2\alpha\xi \sinh \alpha\xi \sin\Omega\right\} \quad \text{(B5)}$$

When k=2 and ℓ=1, Equation (B4) gives a normalized co-spectrum between two adjacent areas in a longitudinal strip such as areas 1 and 2, and if k=3, ℓ = 1, this refers to areas 1 and 3, etc. When k=1. and ℓ=2., this term refers to correlation between two areas in adjacent longitudinal strips such as areas 1 and 5. Therefore, the term $C_N^{32}(\omega)$ would be a calculated normalized co-spectrum between two areas which are separated by one area longitudinally and are in adjacent strips such as areas 1 and 7, Figure 9. Although this method of inputting the normalized co-spectrum appears to involve rather "rash" assumptions, it does permit a means of determining the response with limited wind tunnel data. Also, the method is not as unreasonable as one might think since measured wind tunnel test data do roughly fit the assumption of a simple convected flow pattern, Equation (B2). Therefore, the calculated co-spectrum terms provide a method for use in the computer program, in lieu of sufficient wind tunnel data, if representative decay rates (α, β) are known or can be estimated. This option has been introduced into the response program (Reference 6).

REFERENCES

1. Rainey, A. G., "Progress on the Launch Vehicle Buffeting Problem," J. Spacecraft Rockets, Volume 2, No. 3, May-June 1965.

2. Bieber, R. E., "Prediction of Launch-Vehicle Transonic Buffeting from Wind Tunnel Data," The Shock and Vibration Bulletin, No. 34, Part 2, December 1964.

3. Watts, G. A., "Spacecraft Adapter Response to Fluctuating Pressure," The Shock and Vibration Bulletin, No. 34, Part 2, December 1964.

4. Landahl, Marten T., "A Wave-Guide Model for Turbulent Shear Flow," NASA CR-317, 1965.

5. Davis, R. E., "Random Pressure Excitation of Shells and Statistical Dependence Effect of Normal Mode Response," NASA CR-311, September 1965.

6. Brunkow, A. T., and Davis, R. E., "Conical Shell Deflection and Acceleration Response Program (DARC)," NASA CR-66013, 1965.

7. Weissenburger, J. T., and Davis, R. E., "Fluctuating Pressure Data 7 Percent Mercury-Atlas Configuration," NASA CR-57026, July 1964.

8. Weissenburger, J. T., and Davis, R. E., "Fluctuating Pressure Data 32 Percent Mercury-Atlas Configuration," NASA CR-57027, July 1964.

9. Weissenburger, J. T., and Davis, R. E., "Fluctuating Pressure Data 10 Percent Gemini-Titan Configuration," NASA CR-57028, July 1964.

10. Davis, R. E., "Fluctuating Pressure Data 32 Percent Mercury-Atlas Configuration (Zero Angle-of-Attack)," NASA CR-66004, April 1965.

11. Davis, R. E., "Fluctuating Pressure Data 5.5 Percent Apollo-Saturn Configuration," NASA CR-66005, May 1965. CONFIDENTIAL

12. Shelton, J. D., "Collation of Fluctuating Buffet Pressures for the Mercury-Atlas and Apollo-Saturn Configurations," (Proposed NASA CR).

13. Weissenburger, J. T., and Davis, R. E., "Interim Report on Buffeting Flows Analysis and Experimental Correlation," NASA CR-57024, July 1964.

14. Bendat, J. S., "Probability Functions for Random Responses: Prediction of Peaks, Fatigue Damage, and Catastropic Failures," NASA CR-33, April 1964.

15. McMunn, J. C. and Dick, J. W., "Vibration Analysis of the Ring-Stiffened Conical Shell Gemini Adapter and the Out-of-Plane Ring Vibration Mode," McDonnell Aircraft Corporation, Report No. E137, February 1965.

16. Weissenburger, J. T., "Stiffened Shell Vibrations in the Mercury-Atlas Adapter," Proceeding of the Aero Space Forum I Session, January 1962.

17. Powell, Alan, "On the Estimation of the Generalized Force Due to Random Pressure and on Necessary Modes," J. Acoust, Soc. Am., Volume 36, p. 783, 1964.

18. Kaufman, S., and Hall, D. B., "Static and Dynamic Analysis by a Matrix Force Method," The Shock and Vibration Bulletin, No. 34, Part 2, December 1964.

19. Davis, R. E., Dick, J. W., Suhre, J. R., and Callahan, J. A., "Dynamic Response of Gemini Adapter Module to Aerodynamic Excitation," Proceedings of the AIAA Symposium of Structural Dynamics and Aeroelasticity, Boston, September 1965.

20. Hurty, W. C., "Dynamic Analysis of Structural Systems by Component Mode Synthesis," JPL Technical Report No. 32-520, 1964.

21. Ungar, E. E., "Energy Dissipation at Structural Joints: Mechanisms and Magnitudes," U.S.A.F. (F.D.L.) TDR-64-98, August 1964.

22. McDonnell Aircraft Corporation, Technical Report 045-270, "Dynamic Response Test of Atlas Lox-Dome Vent Valve and McDonnell Aircraft Corporation Adapter Assembly," May 1961.

23. Powell, Alan, "On the Fatigue of Structures Due to Vibrations Excited by Random Pressure Fields," J. Acoust. Soc. Am., Volume 30, No. 12, pp. 1130-1135, December 1958.

24. Bozich, D. J., "Spatial Correlation in Acoustic-Structural Coupling," J. Acoust. Soc. Am., Volume 36, No. 1, January 1964.

25. Coe, C. F., "The Effect of Model Scale on Rigid-Body Unsteady Pressure," Proceedings of RTD/AIA Symposium on Aerolastic and Dynamic Modeling Technology, Part II, September 1963. CONFIDENTIAL

26. McDonnell Aircraft Corporation Report No. 8428, "Mercury-Atlas No. 4 (MA-4) Capsule No. 8A Special Vibration Instrumentation Report," January 1962. CONFIDENTIAL